symmetry

MDPI

Article

Breaking the Symmetry of Cable Structures as an Instrument for Improving Modal Decomposition to Protect Critical Equipment against UWB Pulses

Anton O. Belousov, Natalya O. Vlasova, Viktoriya O. Gordeyeva and Talgat R. Gazizov *

Department of Television and Control, Tomsk State University of Control Systems and Radioelectronics, 634050 Tomsk, Russia; anton.belousov@tu.tusur.ru or ant1lafleur@gmail.com (A.O.B.); ostrolistaya97@mail.ru (N.O.V.); gordeeva.v.110-m1@e.tusur.ru or vikki.gern@gmail.com (V.O.G.)
* Correspondence: talgat@tu.tusur.ru; Tel.: +7-(913)-826-07-24

Abstract: This work presents a detailed, comprehensive study of a new structural design of protective devices with a circular cross-section (CS) (protective cables) for protecting equipment against ultra-wideband (UWB) pulses. Multiconductor structures with 2–5 conductors with and without a protective shield are considered. The disadvantages of using symmetric configurations of protective cables are shown. Their simulation, multivariate analysis, and optimization through heuristic search, as well as evolutionary strategies, were carried out. Optimization was carried out according to the amplitude (to minimize the maximum voltage level at the output of the structures) and time (to maximize the duration of the exciting signal) criteria. The optimization results allowed for increasing the duration and overall attenuation of the exciting UWB pulse. The article shows the possibility of improving the characteristics of such structures through their cascade connection, both among themselves and with strip protective structures. The results of parametric optimization of such structures are presented in the range of real (used in practice) geometric and electrophysical parameters in terms of amplitude and time criteria, as well as the matching criterion. The article also presents the developed prototypes of protective structures with a circular CS of three types: circular 3-conductor cable, flat 3-conductor cable, and circular 4-conductor cable. The experimental results describe how these prototypes were developed and created and confirm the feasibility of these protective structures to decompose the exciting pulse signal, which was previously shown only in simulation. Finally, it is shown that the use of asymmetry in the proposed cable structures can improve their protective characteristics.

Keywords: electromagnetic compatibility; intentional electromagnetic interference; UWB pulse; multiconductor modal filters; microstrip line; circular cross-section; parametric optimization; heuristic search; cascade connection; time response

Citation: Belousov, A.O.; Vlasova, N.O.; Gordeyeva, V.O.; Gazizov, T.R. Breaking the Symmetry of Cable Structures as an Instrument for Improving Modal Decomposition to Protect Critical Equipment against UWB Pulses. *Symmetry* **2022**, *14*, 1228. https://doi.org/10.3390/sym14061228

Academic Editor: Kazuharu Bamba

Received: 15 May 2022
Accepted: 8 June 2022
Published: 13 June 2022

1. Introduction

The functionality and the number of technical devices (TD) of various types and purposes are continuously growing every year. Such growth exacerbates the problem of ensuring electromagnetic compatibility (EMC). It is associated, first of all, with the increasing influence of electromagnetic interference (EMI) of various nature on the operation of critical TD. By critical TD, we mean the devices that operate in the most important sectors of human life. Violation of their normal operation can undermine the stability of their work and lead to various undesirable consequences, from losses in the economic industry to human victims. It is known that EMI sources can cause malfunctions in the automated microprocessor systems, which can ultimately lead to serious system crashes with significant damage. As a rule, the transmission of induced EMI to the microprocessor part of protection and automation devices occurs through control or power cables [1–10]. To ensure the stable operation of electronic systems, it is critical to evaluate the appropriate

characteristics of wires and cables [11]. For example, lightning is a dangerous source of EMI, and its impact can result in TD disruption, leading to serious problems with safety and reliability. Important research in this area is devoted to the characteristics of shielded cables protecting against direct lightning strikes [12–14]. The work [15] describes shielded wires that play an important role in providing communication and protection against EMI. Coaxial cables are widely used in wired communications because of their shielding and mechanical properties. Since some sensitive systems operate in a compact electromagnetic environment, the transmission of safety-related signals is an important task [16]. Cable reliability issues are discussed in [17]. It is known that the cable itself can affect protection systems [18]. In [19], a coaxial low-impedance cable (2–15 Ω) was developed to connect a power system surge protective device. In addition, there are active investigations of EMI effects and their mitigation in flexible flat cables and connectors [20].

It is obvious that the threat of EMI influence on the operation of critical TDs emphasizes the problem of EMC provision [21]. It is known that EMIs are divided into conducted and radiated ones. Special attention should be paid to conducted interference that propagates directly along conductors [22]. Sources of conducted interference can include switching of current circuits, lightning strikes, electrostatic discharge, and intentional ultra-wideband (UWB) pulses [23]. The latter are of the greatest interest due to their peculiarities. For example, the UWB pulses can be represented by ultrashort pulses (USPs) that have a subnanosecond rise time and high voltage levels. Despite their low energy, USPs can cause significant damage to critical TDs, disrupting their operation or even putting them out of action by penetrating critical nodes. Meanwhile, traditional protection devices installed at the TD input have some drawbacks. For example, they are vulnerable to radiation, have a short service life, fail to work at high voltages, or provide insufficient performance. Therefore, in the last decade, there has been an increase in the number of developments that are devoted to protecting equipment against intentional UWB pulses.

Many of these developments are based on modal filtration technology. This technology implies the decomposition of the exciting UWB pulse in transmission lines with inhomogeneous dielectric filling, which is possible due to the difference in mode delays. This technology is effectively used in protective devices called modal filters (MF). The biggest advantages of the MFs include a long service life and radiation resistance that results from the absence of semiconductor components. In addition, their implementation is cheap because their construction employs common and cheap materials. Particularly relevant tasks in the MF design are the search for solutions to reduce the MF weight and size characteristics to expand their application areas and increase the difference in mode delays. The latter can be achieved either by changing the MF length, optimization of its cross-section (CS) parameters, or by using dielectric materials with high relative permittivity. Publication activity of researchers in this direction is quite high [24–29], although they have mainly limited their studies to coupled and multiconductor stripe structures. However, the implementation of the MF in cable structures with a circular CS has practically not been studied, although we consider it relevant. This relevance is explained by the fact that high-frequency transmission systems or measuring devices that employ various cables have become a standard element of TD. In addition, such structures have several advantages compared to MFs based on strip structures: the design flexibility, the length of the structure, and the use of ready-made cable features. Therefore, additional protection in MF-based structures with a circular CS is very important. The purpose of this work is to comprehensively study a new structural design of protective devices with a circular CS (protective cables) for UWB pulse protection.

The design of structures with a circular CS involves the use of circular geometry of the elements and the CS as a whole. Note that the geometric configuration of widely used cables suggests the presence of axial symmetry. However, due to the same electromagnetic coupling between the conductors of symmetric cable structures, the complete decomposition of the exciting USP is practically impossible. The solution is breaking the symmetry of such structures and proceeding to asymmetry.

The article is divided into several sections. Section 2 provides the scientific background. Section 3 describes the methods and approaches used in the work. Section 4 is devoted to the preliminary simulation of a wide range of MFs with a circular CS, and Section 5 is devoted to measurements. Section 6 presents optimization using ES. Section 7 discusses the main results, and Section 8 summarizes them.

2. Scientific Background

The condition for the complete pulse decomposition in an MF of length l is that the total pulse duration t_Σ be less than the minimum modulus of the difference in mode delays [25]:

$$t_\Sigma < l \min |\tau_i - \tau_k|, \quad i, k = 1, \ldots, N, i \neq k, \tag{1}$$

where $\tau_{i(k)}$ is the per-unit-length delay of the $i(k)$ line mode.

An active study of protective structures with a circular CS originates from the use of symmetry in MF geometry [30,31]. Let us consider symmetric MFs with a circular CS in more detail. CSs of eight symmetric MFs with and without a protective shield with (N) 2–5 conductors are presented in Figure 1. Here and further, ε_{ri} is the relative permittivity of the medium, and r_i is the radius of the CS element. The choice of specific parameter values of the considered MFs is complicated. Therefore, we take arbitrary but quite realizable in practice, values of the parameters as initial ones. The parameters of MFs 1–8 are the following: r_1 = 0.9 mm; r_2 = 1.6 mm, r_3 = 3.45 mm; r_4 = 0.95 mm; ε_{r1} = 1; ε_{r2} = 5; ε_{r3} = 10; ε_{r4} = 15. For MF 2, the r_3 value was assumed to be 3.45 mm, and for MF 4 3.6 mm. For MFs 5–7, r_3 = 3.5 mm, and r_5 = 3.6 mm. For MF 8, r_3 = 3.6 mm and r_5 = 3.65 mm. The equivalent circuits of the structures with an MF length (l) equal to 1 m are shown in Figure 2. To ensure the matching of the line with the path, the load (R) values are taken as equal to 50 Ω. As an excitation, we used a source of trapezoidal pulse signals with an EMF of 5 V and rise, fall, and flat top durations of 50 ps. Figure 3 shows the voltage waveforms at the output of MFs 1–8.

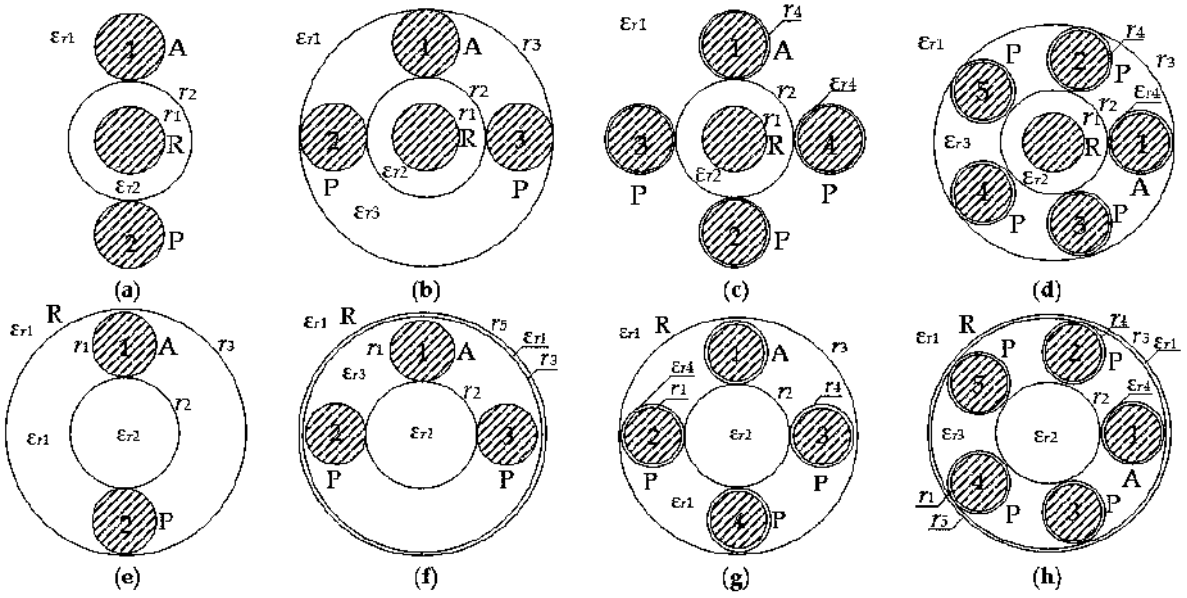

Figure 1. CSs of symmetric (**a**,**e**) MFs 1, 5 with N = 2, (**b**,**f**) MFs 2, 6 with N = 3, (**c**,**g**) MFs 3, 7 with N = 4, (**d**,**h**) MFs 4, 8 with N = 5. Conductors: A—active, P—passive, R—reference.

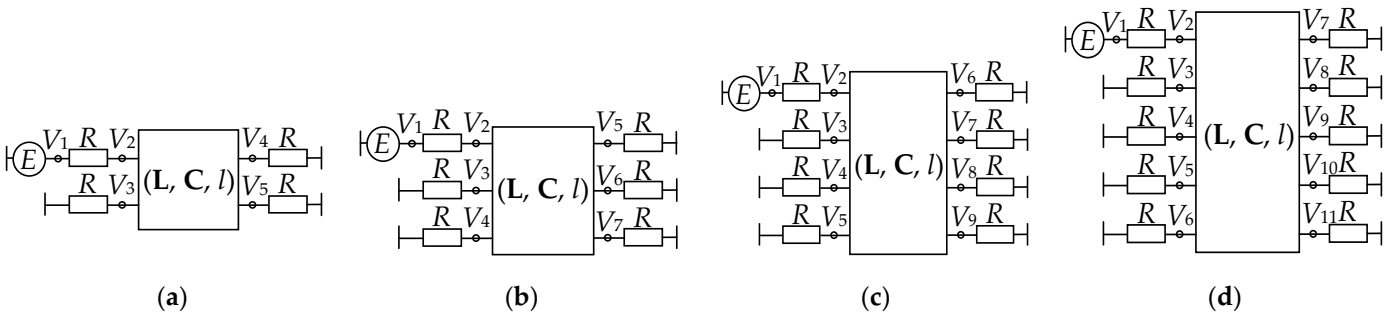

Figure 2. Equivalent circuits of the MFs with (**a**) $N = 2$, (**b**) $N = 3$, (**c**) $N = 4$ and (**d**) $N = 5$.

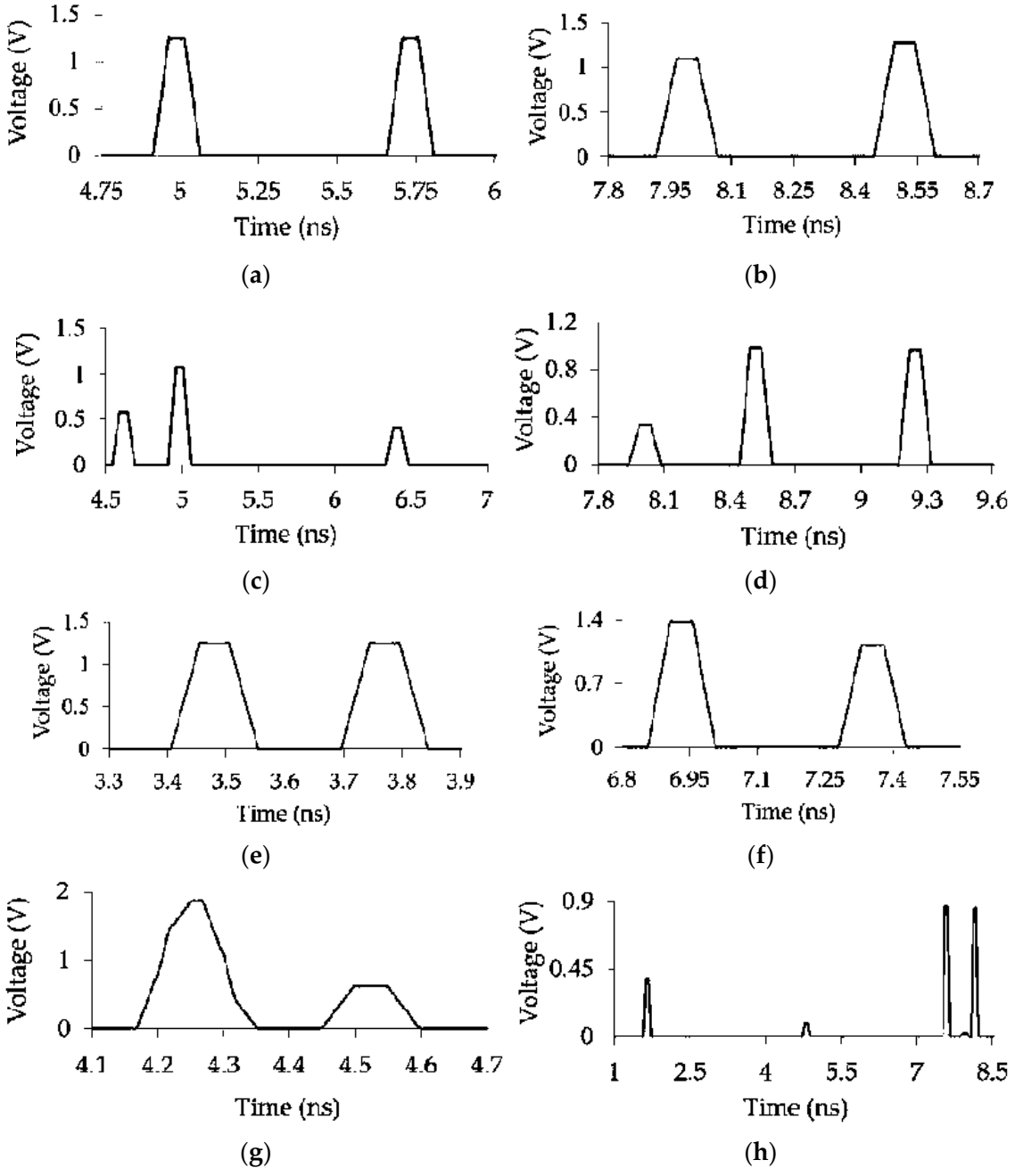

Figure 3. Voltage waveforms at the output of the symmetric (**a**) MF 1, (**b**) MF 2, (**c**) MF 3, (**d**) MF 4, (**e**) MF 5, (**f**) MF 6, (**g**) MF 7, (**h**) MF 8.

From Figure 3, we can see the coincidence of some per-unit-length modal delay (τ_i) values. In the general case, in multiconductor MFs, the number of decomposition pulses (DP) is equal to the number of conductors. This means the simultaneous arrival of modes to the end of the A-conductor (except for the MF with $N = 2$). For example, we can see two and three pulses at the output in MFs 2–4 (assuming full UWB pulse decomposition, we would observe three, four, and five pulses). Obviously, in symmetric MFs with a circular cross-section (for $N > 2$), condition (1) is not satisfied due to the same or similar values of the difference of the per-unit-length modal delays ($\Delta\tau$), as follows from Figure 3. However, the symmetric arrangement of the conductors at $N = 3$ and more will never allow for the complete decomposition of the exciting UWB pulse because the electromagnetic coupling of the active conductor with each of the passive ones is the same. As a consequence, DP overlap and an increase in the resulting amplitudes of the output voltage are inevitable (within this example, up to 1.26 V for MF 2, 1.25 V for MF 3, 0.98 V for MF 4, 1.37 V for MF 6, 1.87 V for MF 7, 0.86 V for MF 8). Note that, in Figure 3g, pulse 1 does not have a trapezoidal shape, which indicates that the values of the $\Delta\tau$ of some pulses (which are in the first pulse in Figure 3g) were very close. Obviously, to achieve a complete decomposition of the exciting UWB pulse, it is necessary to perform optimization and avoid a symmetrical arrangement of conductors in the CS (to distinguish the electromagnetic coupling of an active conductor from passive).

Another resource for improving the protective properties of the MFs under consideration is the possibility of using cascade connection (CC) of protective structures if it is performed with the proper parameter combinations. In addition, parametric optimization of protective structures in the range of real geometric and electrophysical parameters is important. It is necessary to assess if it is possible to decompose the exciting UWB pulse by using the capabilities of real cable structures rather than resorting to expensive materials. At the same time, MFs with a circular CS have so far been optimized only using the heuristic search optimization (HS_{opt}) [32]. This is not always convenient, as it requires a lot of time and concentration on a specific optimization problem from the developer (especially with multicriteria optimization). HS_{opt} involves the implementation of a preliminary multivariate analysis in a range of parameters with one goal—to determine the relationship between the variable parameters and the objective function (OF). Further, the identified features are used to perform optimization. Experience in practical simulation and optimization is relevant in HS_{opt}. Meanwhile, the optimization of protective cables by global optimization methods can eliminate the disadvantages inherent in HS_{opt}. Currently, stripe protective structures with modal decomposition are actively optimized by the genetic algorithm (GA) [33–35] and evolutionary strategies (ES) [36]. Therefore, an important task is to study the possibility of optimizing the MF with a circular CS using evolutionary algorithms. Additionally, the experimental study of this MF deserves special attention. It involves the development and creation of MF prototypes and a comparative analysis of the calculated and measured characteristics.

3. Approaches and Methods

Two, three, four, and five-conductor MFs with a circular CS were taken as the structures under study. Both shielded and unshielded configurations were considered. A 3-conductor microstrip line (MSL) was also used in the CC tasks. All structures were subject to quasi-static simulation, multivariate analysis, and parametric optimization.

The simulation took several steps. First, we created geometric models of the MF CS. Then, we calculated the matrices of per-unit-length coefficients of electrostatic (**C**) and electromagnetic (**L**) inductances. To calculate the responses, we made a circuit, set loads and excitation, and then calculated the time responses in the range of parameters. The simulation was performed in the TALGAT system, which gives acceptable accuracy and does not require high computational costs [37]. The validation of the system has been repeatedly demonstrated in various scientific publications, for example [38]. The values of the loss matrices in the conductors (**R**) and dielectrics (**G**) were taken to be zero in the

lossless simulation. To calculate the elements of matrix **G**, we used the fixed values of the relative permittivity and the tangent of the dielectric loss angle in the lossy simulation. The elements of matrix R were calculated taking into account the skin effect, proximity effect, and loss in the ground plane, according to the method from [39].

Optimization by HS_{opt} was performed according to three criteria. The first one is the amplitude criterion to minimize the maximum voltage at the MF output. The second one is the time-interval criterion to equalize the time intervals between the DPs at the MF output. The third one is the range-time criterion to maximize the duration of the DPs at the MF output. In addition, the optimization implied the matching between the MF and the path. The MFs were optimized using a modified ES algorithm with constraints, which allows you to set the range of optimized parameters [40]. The idea of the modified algorithm is that a value that exceeds the specified range is replaced by a random number in that range. Thus, the algorithm does not allow the optimized parameters to go beyond the permissible values and, at the same time, introduces an element of randomness. It positively affects the finding of the global extremum (as compared to the traditional ES algorithm). Finally, ES optimization was performed according to the amplitude criteria.

In the full-scale experiment, the excitation was a real pulse signal received by taking the derivative of a step excitation obtained with a Tektronix DSA 8300 digital strobe oscilloscope. Frequency dependences of $|S_{21}|$ of the prototypes were measured using a vector electric circuit analyzer «Panorama» P4226.

4. Simulation and Multivariate Analysis of Protective Structures with a Circular Cross-Section

4.1. Optimization of the Structures

4.1.1. Parametric Optimization of Unshielded Structures

As noted earlier, the symmetric arrangement of the conductors does not allow for complete decomposition of the exciting UWB pulse, so it is reasonable to perform optimization to eliminate this non-deficiency. We will consider MFs 2–4 because their CSs correspond to the commonly available cable grades, as shown in Figure 1b–d. For example, cable PBPPg (PUGNP) is widely used for switching lighting equipment and connecting low-power devices. Another example is a widely used cable for energy transmission and distribution. It has PVC-insulated conductors and is commonly used in industrial premises, power plants, distribution, and lighting devices, as well as in ordinary households as wiring. MF CSs after the parametric optimization by HS_{opt} according to the amplitude, the time-interval, and the minimum and maximum-time criteria are shown in Figure 4. Optimization of MF 1 was not required because it has only one active and one passive conductor. Hence, the exciting UWB pulse is completely decomposed at the output of such an MF.

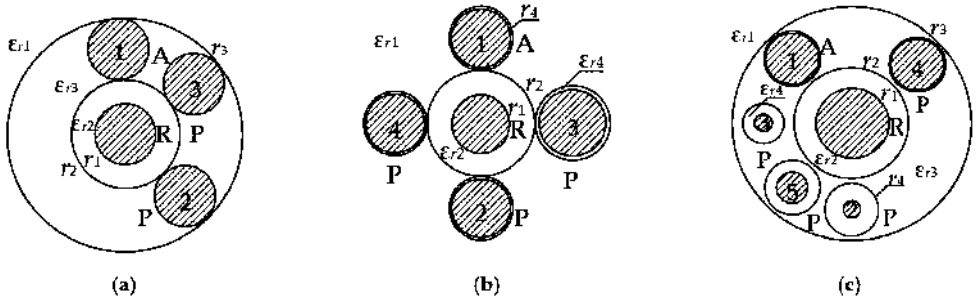

Figure 4. CSs of (**a**) MF 2, (**b**) MF 3, and (**c**) MF 4 after HS_{opt}.

As a result of MF 2 optimization, the following values were obtained: $\varepsilon_{r1} = 1$; $\varepsilon_{r2} = 5$; $\varepsilon_{r3} = 19$; $r_1 = 0.9$ mm for the reference conductor and conductors 1 and 2; $r_1 = 0.89$ mm for conductor 3; $r_2 = 1.6$ mm; $r_3 = 3.45$ mm. The R values were taken as equal to 35 Ω to ensure the matching of the line with the path. The excitation was taken the same as in Section 2. First, in order to establish various coupling between the conductors in order to obtain a

complete decomposition of the exciting UWB pulse, the arrangement of conductors 2 and 3 in the internal dielectric filling was changed. The optimization process revealed that the change in ε_r value of the external dielectric allows one to increase the time intervals between pulses 1 and 2. A slight change of r_1 value for conductor 3 leads to an increase in the U_2 value, thereby making it possible to align the maximum voltages of the DPs. As a result, a complete decomposition of the exciting pulse into three pulses of lower maximum voltages was achieved, and the amplitudes of the DPs were equalized.

As a result of MF 3 optimization, the following values were obtained: $\varepsilon_{r1} = 1$; $\varepsilon_{r2} = 3$; $\varepsilon_{r4} = 60$ around conductors 1 and 3; $\varepsilon_{r4} = 120$ around conductor 2; $\varepsilon_{r4} = 20$ around conductor 4; $r_1 = 0.9$ mm for the reference conductor and conductors 1, 2, and 4; $r_1 = 1$ mm for conductor 3; $r_2 = 1.6$ mm; $r_4 = 0.95$ mm for conductors 1, 2, and 4; $r_4 = 1.1$ mm for conductor 3. The R values were taken as equal to 68 Ω to ensure the matching of the line with the path. It was found that an increase in the r_1 values for conductor 3 and r_4 for conductor 3 leads to a slight decrease in the amplitude of U_2. An increase in the ε_{r4} around conductor 1 leads to an increase in the U_2 and a slight decrease in the time interval between pulses 1 and 2 and a significant increase in the U_2, and also a decrease in the time interval between pulses 2 and 3. An increase in the ε_{r4} around conductor 2 leads to an increase in the U_1, a significant decrease in the U_2, and a slight decrease in the U_3. As a result, complete decomposition of the exciting UWB pulse signal into four pulses of lower maximum voltages was achieved. To maximize the time intervals between DPs, the ε_{r4} value around conductor 4 was slightly increased, which also led to an increase in the U_1 and a decrease in the U_2. As a result of optimization, a complete UWB pulse decomposition was achieved, and the maximum voltages of the first three pulses were equalized.

As a result of MF 4 optimization, the following values were obtained: $\varepsilon_{r1} = 1$; $\varepsilon_{r2} = 70$; $\varepsilon_{r3} = 6$; $\varepsilon_{r4} = 5$ around conductor 1; $\varepsilon_{r4} = 3$ around conductor 2; $\varepsilon_{r4} = 10$ around conductor 3; $\varepsilon_{r4} = 27$ around conductor 4; $\varepsilon_{r4} = 15$ around conductor 5; $r_1 = 1.22$ mm for the reference conductor; $r_1 = 0.9$ mm for conductors 1 and 4; $r_1 = 0.3$ mm for conductors 2 and 3; $r_1 = 0.55$ mm for conductor 5; $r_2 = 1.9$ mm; $r_3 = 4$ mm; $r_4 = 0.95$ mm for conductors 1, 4, and 5; $r_4 = 0.92$ mm for conductor 2; $r_4 = 0.69$ mm for conductor 3. The R values were taken as equal to 33 Ω to ensure the matching of the line with the path. Changing the ε_{r3} value made it possible to slightly increase the time intervals between pulses 2, 3, and 4. Changing the arrangement of passive conductors made it possible to reduce U_1 and increase U_2. It also allowed us to decrease the time interval between pulses 4 and 5, which also led to a slight decrease in the time interval between pulses 1 and 2, and 3 and 4. A decrease in the r_1 values for passive conductors, as well as an increase in the r_1 values for the active conductor and the r_4 value for all conductors, made it possible to reduce U_2 and increase U_5. However, these changes also uniformly reduced the time intervals between the first four pulses. A decrease in the ε_{r4} values around conductors 1 and 2 made it possible to reduce U_3. An increase in the ε_{r4} values around conductors 3, 4, and 5 made it possible to decrease U_5, increase the time intervals between the DPs, and equalize the maximum voltages of the first four DPs.

The MF output characteristics after optimization are summarized in Table 1. In addition, in Table 1, for clarity, the MF 1 output characteristics are summarized as well. The $\Delta\tau_i$ values show that a complete decomposition of the exciting UWB pulse was achieved in all MFs. The voltage waveforms at the MFs 2–4 output after optimization are shown in Figure 5.

The minimum $\Delta\tau_i$ values for MFs 1–4 are 0.75, 1.72, 0.25, and 0.58 ns/m, which demonstrates the complete decomposition of the exciting UWB pulse. The maximum amplitudes of the DPs are 1.25, 0.73, 0.67, and 0.55 V (which is 2, 3, 3.58, and 4.18 times less than the U_{in}). Analyzing the results, one can say that the total duration of the exciting UWB pulse (with allowance for the partial superposition of the rise and the fall of adjacent DPs) can be increased by up to 0.744, 1.71, 0.249, and 0.579 ns for MFs 1–4, respectively, with the same attenuation coefficient. According to condition (1), the duration of excitation (150 ps) is much less than the minimum mode delay difference in the considered MFs (Table 1 at

l = 1 m). Thus, condition (1) is ensured in these MFs (in contrast to symmetric MFs with a circular CS).

Table 1. Voltage waveform characteristics at the output of MF 1 without optimization and MFs 2–4 after HS_{opt} (where U_{in}—input voltage, U_i—DP amplitudes).

MF	U_{in}, V	DP Amplitudes, V					Differences in Per-Unit-Length Delays Δτ, ns/m			
		U_1	U_2	U_3	U_4	U_5	$\Delta\tau_1$	$\Delta\tau_2$	$\Delta\tau_3$	$\Delta\tau_4$
1	2.49	1.24	1.25				0.75			
2	2.2	0.73	0.72	0.73			1.77	1.72		
3	2.4	0.65	0.66	0.67	0.45		0.4	0.25	0.5	
4	2.3	0.54	0.54	0.54	0.55	0.25	0.58	0.93	1.24	0.78

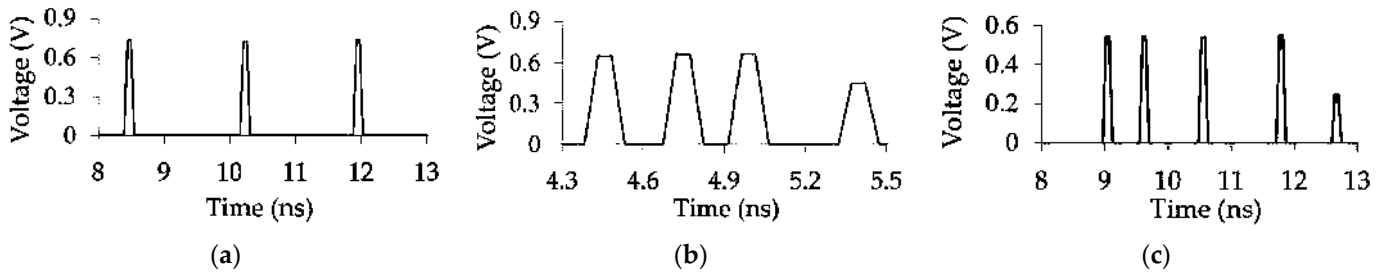

Figure 5. Voltage waveforms at the output of (**a**) MF 2, (**b**) MF 3, and (**c**) MF 4 after HS_{opt}.

4.1.2. Parametric Optimization of Shielded Structures

We consider the shielded MFs with a circular CS discussed in [41]. Their CSs before optimization are shown in Figure 1e–h with initial parameter values: r_1 = 0.9 mm; r_2 = 1.6 mm, r_3 = 3.5 mm; r_4 = 0.95 mm; r_5 = 3.6 mm; ε_{r1} = 1; ε_{r2} = 5; ε_{r3} = 10; ε_{r4} = 15. The CSs of MFs 5–8 with parameters after HS_{opt} are shown in Figure 6, and the voltage waveforms at the output of MFs 5–8 after optimization are shown in Figure 7. The output characteristics of MFs after optimization are summarized in Table 2.

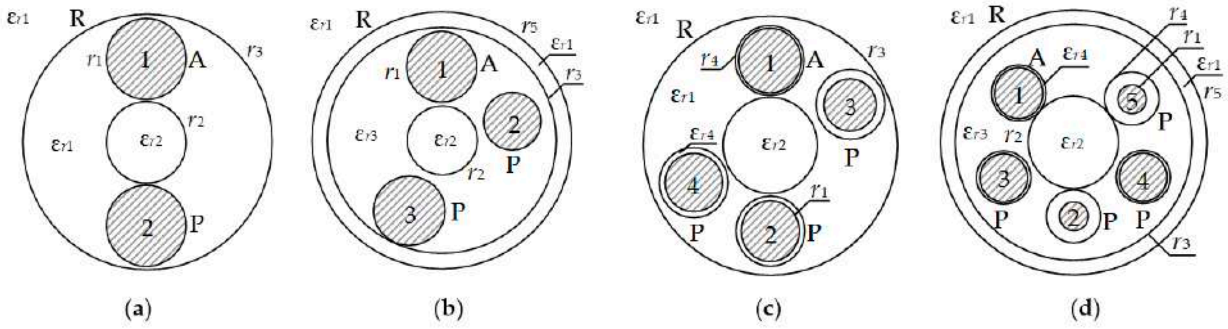

Figure 6. CSs of (**a**) MF 5, (**b**) MF 6, (**c**) MF 7, and (**d**) MF 8 after HS_{opt}.

In spite of the fact that the complete decomposition of the exciting UWB pulse at the MF 5 output is achieved at the initial parameters, its characteristics could be improved by increasing the time intervals between the DPs (achieved by reducing the r_2 value). After optimization, the following parameter values were obtained: ε_{r1} = 1; ε_{r3} = 10; r_1 = 0.9 mm; r_2 = 0.9 mm; r_3 = 2.8 mm. The R value was taken as equal to 18 Ω to match the MF with the path. After optimization of MF 6, the r_2 value decreased, which resulted in an increase in the time intervals between the DPs. The complete decomposition of the exciting UWB pulse was achieved by changing the location of the passive conductors relative to the active one, as well as by changing the ε_{r3} value. After optimization, we also equalized the amplitudes of all DPs. The following parameter values were obtained: ε_{r1} = 1; ε_{r2} = 5; ε_{r3} = 23; r_1 = 0.9 mm for conductors 1 and 3; r_1 = 0.73 for conductor 2;

r_2 = 0.9 mm; r_3 = 3.3 mm; r_5 = 3.7 mm. The R value was taken as equal to 20 Ω to match the line with the path. After optimization of MF 7, the values of ε_{r2}, ε_{r4} around conductors 1, 2, and 4, as well as the values of r_1 for conductors 2, 3, and 4 and their location were changed. After optimization, the complete decomposition of the exciting UWB pulse into four pulses of lower amplitudes was achieved. The following parameter values were obtained: ε_{r1} = 1; ε_{r2} = 60; ε_{r4} = 24 around conductor 1; ε_{r4} = 11 around conductor 2; ε_{r4} = 15 around conductor 3; ε_{r4} = 5 around conductor 4; r_1 = 0.9 mm for conductor 1; r_1 = 0.8 mm for conductors 2 and 4; r_1 = 0.7 mm for conductor 3; r_2 = 1.3 mm; r_4 = 0.95 mm. The R value was taken as equal to 31 Ω to match the MF with the path. After optimization of MF 8, the values of ε_{r2}, ε_{r4} around conductors 1–5, were changed, as well as the values of r_1 and their location for conductors 2–5. The following parameter values were obtained: ε_{r1} = 1; ε_{r2} = 120; ε_{r3} = 5; ε_{r4} = 4 around conductor 1; ε_{r4} = 20 around conductor 2; ε_{r4} = 3 around conductor 3; ε_{r4} = 55 around conductor 4; ε_{r4} = 42 around conductor 5; r_1 = 0.9 mm for conductor 1; r_1 = 0.5 mm for conductor 2; r_1 = 0.8 mm for conductor 3; r_1 = 0.82 mm for conductor 4; r_1 = 0.5 mm for conductor 5; r_2 = 1.55 mm; r_3 = 4.6 mm; r_4 = 0.95 mm; r_5 = 5.1 mm. The R value was taken as equal to 29 Ω to match the MF with the path.

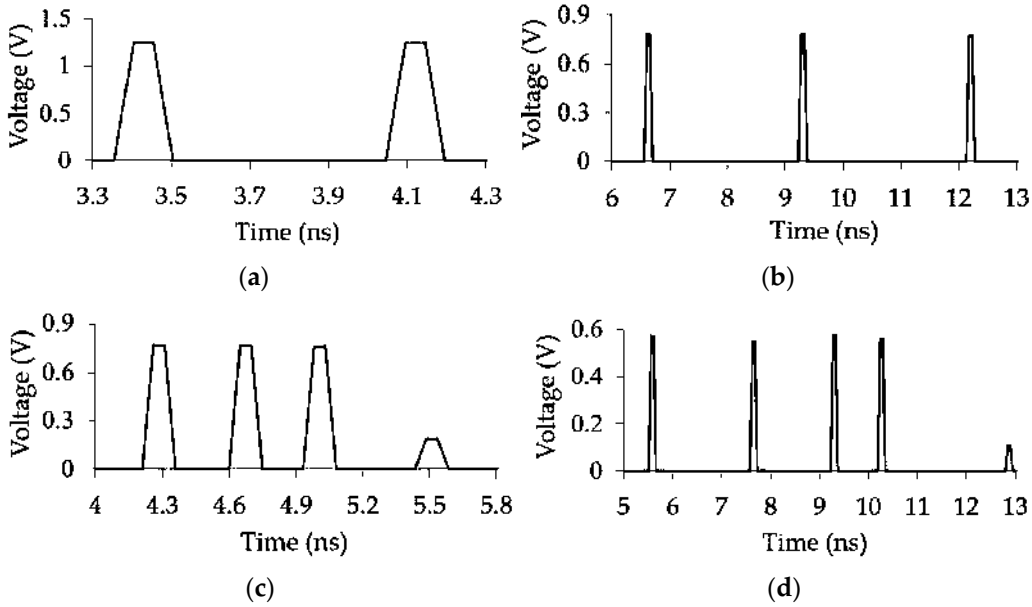

Figure 7. Voltage waveforms at the output of (**a**) MF 5, (**b**) MF 6, (**c**) MF 7, and (**d**) MF 8 after HS_{opt}.

Table 2. Voltage waveform characteristics at the output of MF 1 before optimization and MFs 5–8 after HS_{opt} (where U_{in}—input voltage, U_i—DP amplitudes).

MF	U_{in}, V	DP Amplitudes, V					Differences in Per-Unit-Length Delays Δτ, ns/m			
		U_1	U_2	U_3	U_4	U_5	$\Delta\tau_1$	$\Delta\tau_2$	$\Delta\tau_3$	$\Delta\tau_4$
5	2.49	1.248	1.249				0.69			
6	2.46	0.78	0.78	0.78			2.67	2.9		
7	2.47	0.77	0.77	0.76	0.19		0.39	0.34	0.5	
8	2.46	0.57	0.55	0.57	0.56	0.12	2.07	1.65	0.9	2.5

Figure 7 shows that 2–5 pulses of lower amplitudes come to the end of MFs 2–5. It follows from Table 2 that the minimum $\Delta\tau_i$ values for MFs 5–8 are 0.69, 2.67, 0.34, and 0.9 ns/m. Therefore, for MFs 5–8, it is possible to increase the exciting pulse duration to 0.681, 2.664, 0.324, and 0.89 ns with the same attenuation coefficient. Thus, Figure 7 shows the complete decomposition of the exciting UWB pulse in all MFs. This is confirmed by the results from Table 2, which, among other things, show the matching of MFs 5–8 with the path (the U_{in} values are close to half the EMF amplitude in all MFs).

4.2. Cascade Connection of Modal Filters

In this subsection, we explore the possibility of improving the performance of multiconductor MFs (with a circular CS and based on MSL) by cascading them. It is known [42] that each pulse is successively divided into two pulses of smaller amplitudes when segments of coupled lines are connected in cascade. In other words, connecting another segment to the line segment leads to the fact that pulse 1 is decomposed into pulse 1.1 and pulse 1.2, while pulse 2 is decomposed into pulse 2.1 and pulse 2.2. These pulses will not coincide with each other in time if the mode delay difference of the second segment is at least twice as big as that of the first one. The result is the sequence of pulses 1.1, 2.1, 1.2, 2.2. Consequently, the CC of n segments will lead, under certain conditions, to the decomposition into 2^n pulses, which is possible with a successive doubling or shortening of the lengths of the connected line segments.

For a structure of n segments of connected lines, the length of the k-th segment is defined as:

$$l_k = l(2k - 1), k = 1, \ldots, n, \quad (2)$$

with the total length of the structure

$$L_n = l(2_n - 1). \quad (3)$$

The resulting formulas (2) and (3) relate the number and lengths of coupled line segments for pulse decomposition with given parameters [42]. We considered the above conditions only in relation to the CC of segments of coupled lines of the same type, while this issue was not touched upon for structures that were different (in terms of CSs).

For the study, we selected 3-conductor MFs: with a circular CS and an MSL. Figures 4a and 8a show their CSs, where w is the width of the conductors, d is the distance from the edge of the MSL to the nearest conductor, s is the separation between the conductors, t is the conductor's thickness, and h is the substrate thickness. In the simulation, the source of UWB pulses is represented by an ideal trapezoidal signal source with 1 V EMF and rise, fall, and flat top durations of 50 ps, so that the total duration was 150 ps. Figure 8b,c show the equivalent circuits of the CSs, and Figure 8d,e show the voltage waveforms at the beginning and end of single-segment MFs with a circular CS and an MSL. We considered a multiconductor MF with a circular CS in Section 4.1. This structure for $N = 3$ is shown in Figure 4a. We also performed the optimization of this MF by HS_{opt} for amplitude, interval-time, and range-time criteria (see Section 4.1). Equal amplitudes of the DPs were achieved, and a 3-time attenuation of the output signal was obtained compared to $U_{in} = 0.44$ V (recalculated with respect to the data from Table 1 when excitation was 1 V). An MF based on an MSL was previously considered in [43] and is a 3-conductor transmission line (Figure 8a). The parameters of the MSL are taken as follows: $\varepsilon_{r1} = 1$; relative permittivity of the substrate $\varepsilon_{r5} = 4.5$; $w_{1–3} = 1$ mm; $t = 0.178$ mm; $h = 0.323$ mm; $s_1 = 0.011$ mm; $s_2 = 0.09$ mm. As a result, the maximum attenuation of the output voltage was 2.6 times compared to $U_{in} = 0.42$ V (Figure 8d). Four options for CC of MFs were considered and are described in detail below. When simulating CCs 1–4, the R values were taken based on the conditions for matching the MF with the path (the U_{in} value was equal to half the EMF of the source). The lengths of the segments l_i were optimized by HS_{opt} to achieve a complete decomposition of the UWB pulse.

Figure 8b shows the equivalent circuit of CC 1 and CC 2. CC 1 includes two segments of the circular CS MF from Figure 4b. CC 2 includes an MF segment with a circular CS (Figure 4b) and an MSL (Figure 8a). As a result of optimization, the l_i values of $l_1 = 0.1$ m and $l_2 = 0.3$ m for CC 1, and $l_1 = 0.1$ m and $l_2 = 0.5$ m for CC 2 were chosen. To ensure the matching of the line with the path, the load's R values in this subsection are taken as equal to 25 Ω. Figure 9a,b show the voltage waveforms at the output of CC 1 and CC 2. Figure 9a shows that three pulses arrive at the output of segment 1 (node V_5 in Figure 8b) with a maximum amplitude of 174 mV and a minimum delay difference $\Delta t_{min} = 0.02$ ns. The output of segment 2 (node V_{10} in Figure 8b) receives nine pulses with a maximum

amplitude of 57 mV and Δt_{min} = 0.03 ns, which is 8.9 times less than the level U_{in} = 510 mV. Figure 9b shows that three pulses arrive at the output of segment 1 with a maximum amplitude of 141 mV and Δt_{min} = 0.02 ns. Nine pulses with a maximum amplitude of 55 mV and Δt_{min} = 0.055 ns come to the output of segment 2, which is 9.4 times less than the U_{in} = 510 mV.

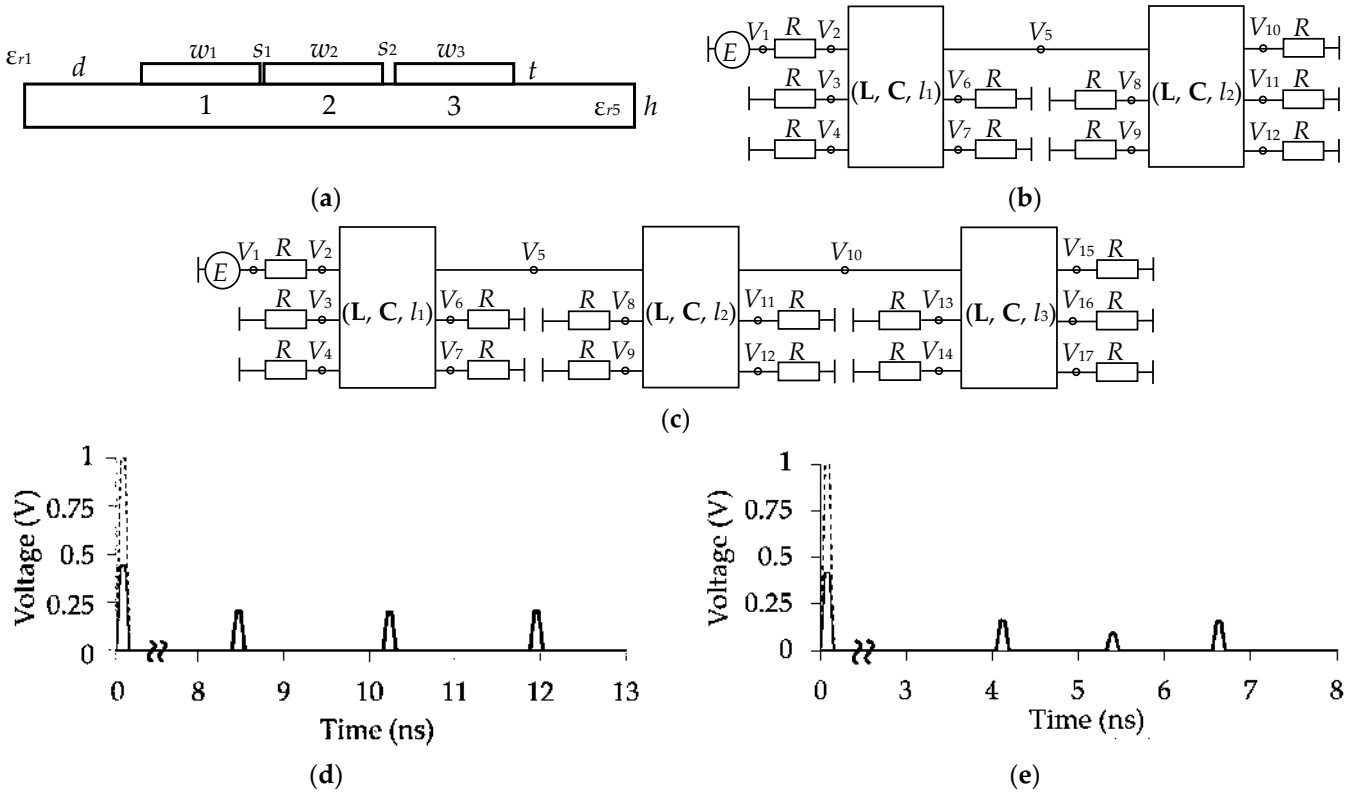

Figure 8. (**a**) CS of a 3-conductor MSL, equivalent circuits of (**b**) CC 1 and 2, (**c**) CC 3 and 4, and output voltage waveforms of the single (**d**) circular MF and (**e**) MSL.

Figure 8c shows the equivalent circuit of CC 3 and CC 4. CC 3 includes two MFs with a circular CS, between which there is the MSL segment. CC 4 includes three segments of the MF with a circular CS. As a result of optimization, the l_i values were chosen to equal l_1 = 0.1 m, l_2 = 0.5 m, l_3 = 1.1 m for CC 3, and l_1 = 0.1 m, l_2 = 0.3 m, l_3 = 1.2 m for CC 4. Figure 9c shows that three pulses arrive at the output of segment 1 (node V_5 in Figure 8c) with a maximum amplitude of 141 mV and Δt_{min} = 0.02 ns. Nine pulses with a maximum amplitude of 56 mV and Δt_{min} = 0.05 ns propagate to the output of segment 2 (node V_{10} in Figure 8c). The output of segment 3 (node V_{15} in Figure 8c) receives 27 pulses with a maximum amplitude of 22.3 mV and Δt_{min} = 0.01 ns, which is 23.1 times less than the U_{in} = 515 mV. Figure 9d shows that three pulses arrive at the output of segment 1 with amaximum amplitude of 175 mV and Δt_{min} = 0.02 ns. Nine pulses with a maximum amplitude of 58 mV and Δt_{min} = 0.05 ns come to the output of segment 2. A total of 27 pulses with a maximum amplitude of 20.2 mV and Δt_{min} = 0.01 ns come to the output of segment 3, which is 25.5 times less than the U_{in} = 515 mV.

Tables S1–S4 (in Supplementary Materials) show the main characteristics of CCs 1–4 after optimization. The amplitudes of the DPs and delays at the output of segments 1 (node V_5), 2 (V_{10}), and 3 (V_{15}) are also presented.

Tables S1–S4 show the coincidence of the U_i and t_i values at the V_5 nodes in pairs in CC 1 and CC 4, as well as in CC 2 and CC 3. This is because the sequence of segments 1 and 2 is the same: segments 1 and 2 are MFs with a circular CS (CC 1 and CC 4), and segments 1 and 2 are MFs with a circular CS and MSL (CC 2 and CC 3). In addition, we can see that in

the separately indicated CC, the pulses at the output of segment 2 (node V_{10}) have U_i and t_i values that are close. Note are due to the partial mismatch of the modes in the CC of the transmission line segments; there is a consistent increase in the amplitudes of individual pulses in individual nodes. For example, in the V_{10} node of CC 1, we observe an increase in the pulse amplitude from 33 mV for pulse 1 to 57 mV for pulse 9. The phenomenon of mismatch of individual mode pulses leads to different U_i values in individual nodes. It is especially clearly observed for CCs 2 and 3, where two protective devices with different CSs are connected. It can be seen from the minimum differences in mode delays Δt_{min} that at the V_5 node in all CCs, this value is 0.02 ns, V_{10} is 0.03 ns, and V_{15} is 0.01 ns. This indicates a partial pulse overlapping at the CC output, which leads to an increase in the maximum level of the output voltage in the node (V_{15}) when simulating CC 3 (Figure 9c). However, the obtained results indicate the possibility of improving the protective characteristics of individual MFs that function separately. This can be achieved by cascading them with other MFs that have different geometric configurations.

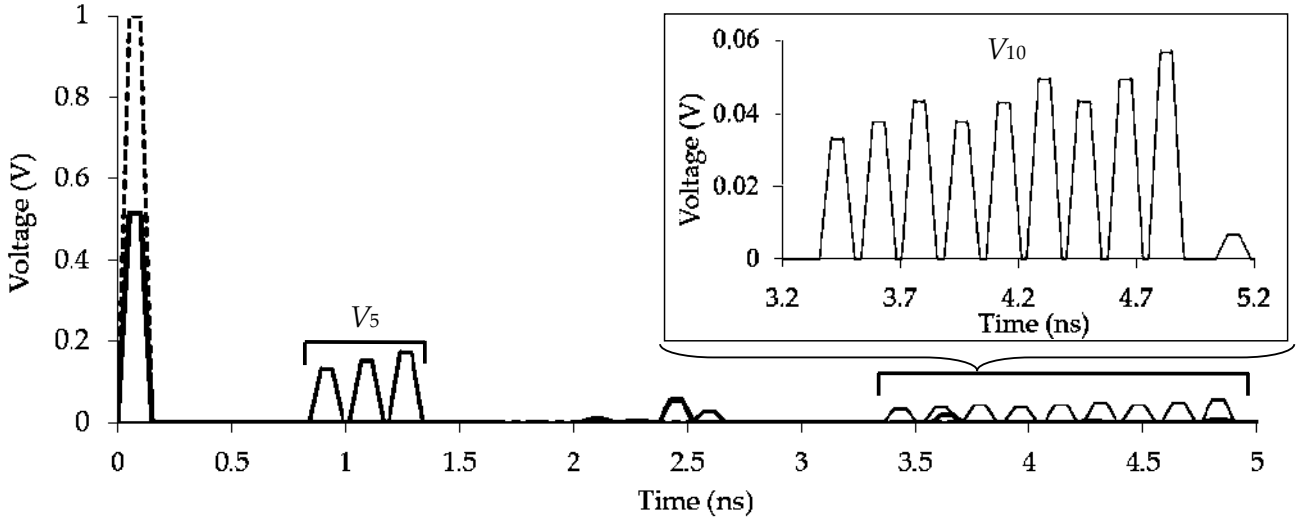

(**a**)

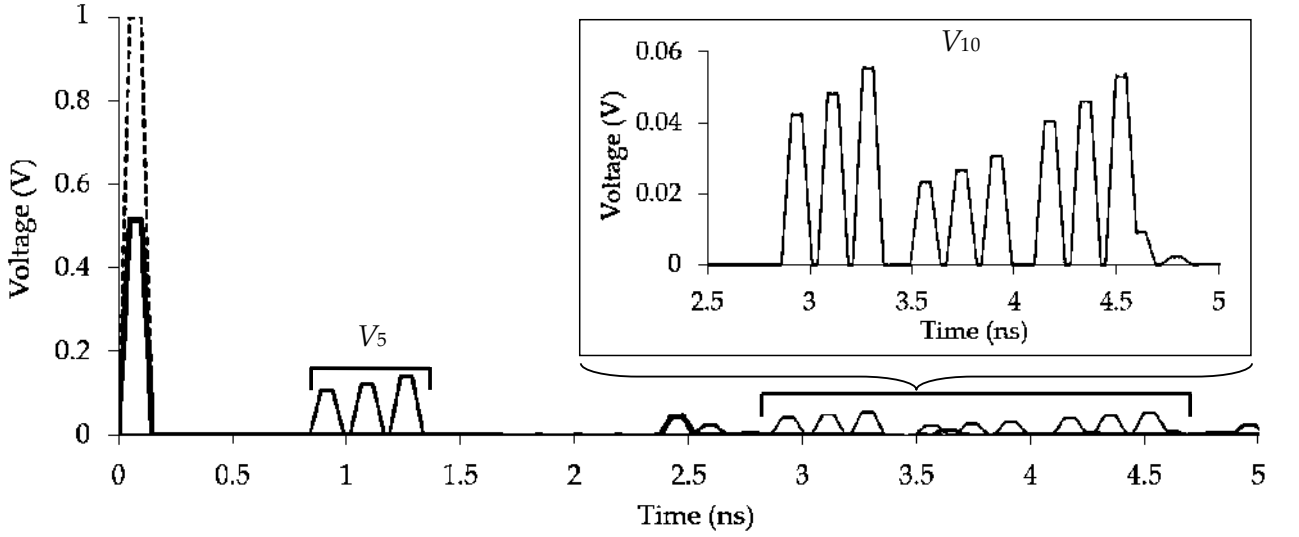

(**b**)

Figure 9. *Cont.*

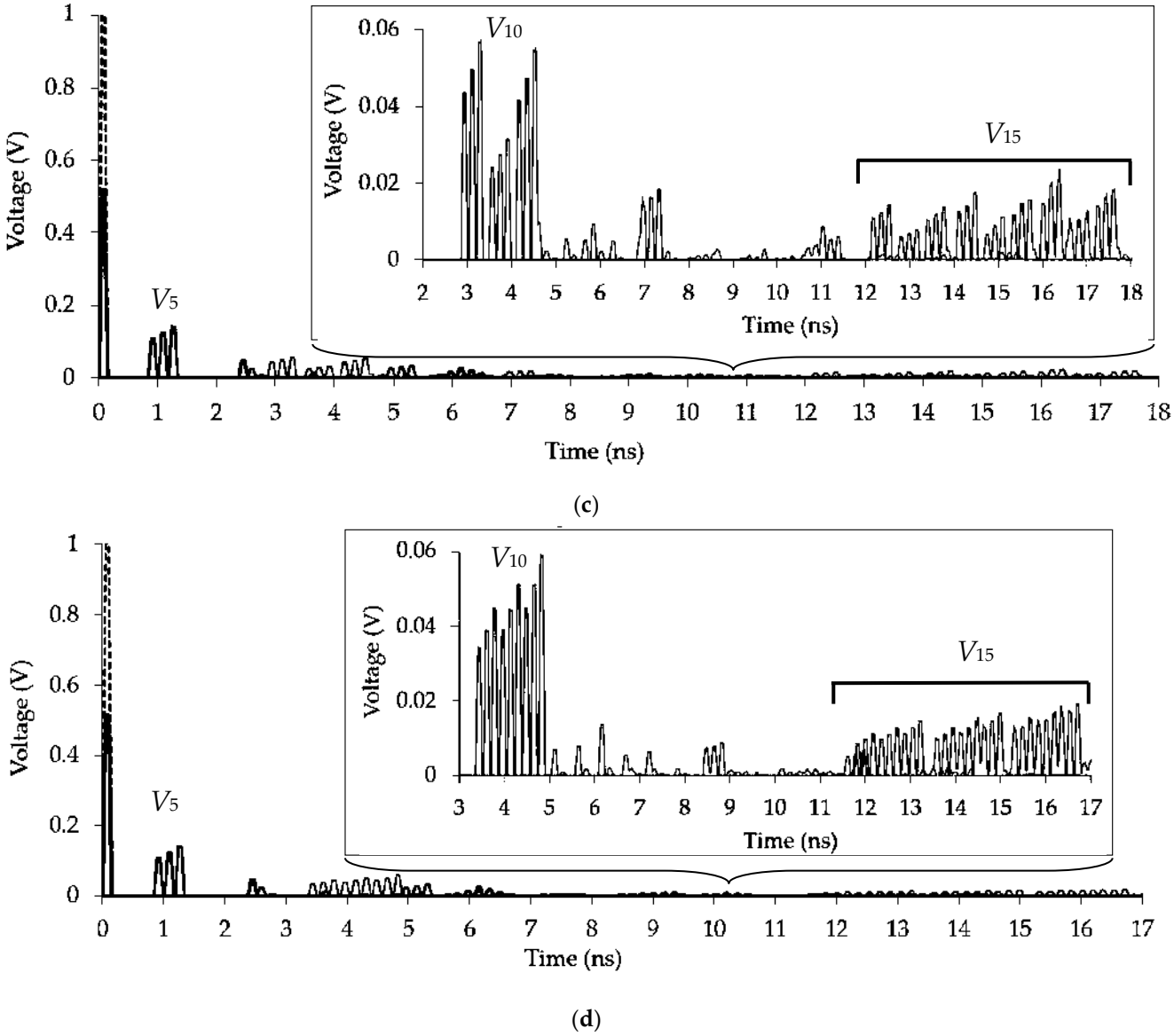

Figure 9. Output voltage waveforms of (**a**) CC 1, (**b**) CC 2, (**c**) CC 3, and (**d**) CC 4 after optimization.

4.3. Parametric Optimization of Modal Filters in the Range of Real Geometric and Electrophysical Parameters

In this subsection, we present the results of simulating MFs with a circular CS in the range of real parameters when they are designed in the shield and without it [31,41,44]. The possibility of achieving a complete decomposition of the exciting UWB pulse is evaluated at real geometrical and electrophysical parameters of the MF. It is important to implement the protective cable prototype. The study considers eight 2 and 3-conductor MFs with circular CSs, as shown in Figure 10. The choice of the optimized parameter range was conditioned by the typical characteristics of cables in terms of their geometrical and electrophysical parameters. Thus, during the optimization, the radius of the conductors varied within 0.5–2.15 mm, the internal insulation (around the reference conductor or in the form of a central dielectric core) and the internal insulation around the conductors were 0.5–1.6 mm, the external insulation was 3.55–9.75 mm, and the relative permittivity of the insulating materials was 2.4–5.5 (with values of the dielectric loss tangent ($tg\delta_i$) 0.007–0.017).

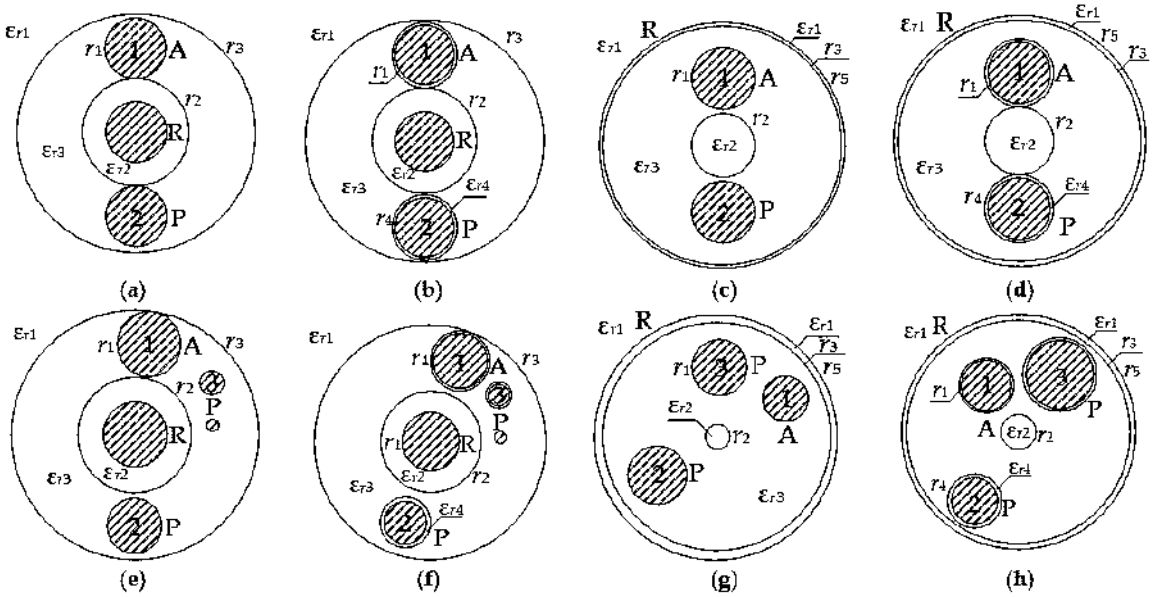

Figure 10. CSs of (**a**) MF 1, (**b**) MF 2, (**c**) MF 3, (**d**) MF 4, (**e**) MF 5, (**f**) MF 6, (**g**) MF 7, and (**h**) MF 8 after HS_{opt}.

Eight different MFs were investigated: MFs 1–4 with $N = 2$ and MFs 5–8 with $N = 3$. Let us describe them in more detail. MF 1 (Figure 10a) is a reference dielectric-coated conductor. Conductors 1 and 2 are located on the outside of the dielectric, and the entire structure is in dielectric insulation. MF 2 (Figure 10b) is similar to MF 1, but conductors 1 and 2 are in an individual dielectric filling. MF 3 (Figure 10c) is the same as MF 1 but with an external shield and dielectric instead of a center conductor. MF 4 (Figure 10d) is the same as MF 3, but conductors 1 and 2 are in individual dielectric insulation. MFs 5–8 from Figure 10e–h are similar to MFs 1–4, but they are distinguished by having conductor 3. We set the R values equal to 50 Ω when simulating MFs 1–8. As an input excitation, we used a source of trapezoidal pulse signals with an EMF equal to 5 V and a total duration of 150 ps. The equivalent circuits of MFs that are 1 m long are shown in Figure 2a,b.

The parameters after MFs 1–4 optimization are presented in Table 3, and MFs 5–8–in Table 4 (where C_R is the reference conductor and C_i is the number of the signal conductor). The calculated voltage waveforms at the output of MFs 1–8 after HS_{opt} are shown in Figures 11 and 12. Table 5 shows the main characteristics of MFs 1–8 after parametric optimization by HS_{opt} when simulating them without considering losses, and Table 6 with considering losses.

Table 3. Parameters of MFs 1–4 after HS_{opt}.

MF	r_i, mm										ε_{ri} and $tg\delta_i$											
	r_1				r_2	r_3	r_4			r_5	ε_{r1}	ε_{r2}	$tg\delta_2$	ε_{r3}	$tg\delta_3$	C_1		C_2		C_3	
	C_R	C_1	C_2	C_3			C_1	C_2	C_3							ε_{r4}	$tg\delta_4$	ε_{r4}	$tg\delta_4$	ε_{r4}	$tg\delta_4$
1	0.9	0.9	0.77	0.35	1.6	3.45					1	4.2	0.07	4.2	0.07						
2	0.9	0.9	0.7	0.37	1.6	3.7	0.95	0.82	0.42		1	4.2	0.07	4.2	0.07	2.4	0.07	2.4	0.07	2.4	0.07
3	0.9	0.9	1.18	1.13	0.5	4.5				4.8	1	2.4	0.07	5.5	0.017						
4	0.9	0.9	0.82	1.2	0.6	3.9	0.95	0.95	1.3	4.1	1	4.2	0.07	2.4	0.07	5.5	0.017	5.5	0.017	4.2	0.07

Table 4. Parameters of MFs 5–8 after HS_{opt}.

MF	r_i, mm										ε_{ri} and $tg\delta_i$											
	r_1				r_2	r_3	r_4			r_5	ε_{r1}	ε_{r2}	$tg\delta_2$	ε_{r3}	$tg\delta_3$	C_1		C_2		C_3	
	C_R	C_1	C_2	C_3			C_1	C_2	C_3							ε_{r4}	$tg\delta_4$	ε_{r4}	$tg\delta_4$	ε_{r4}	$tg\delta_4$
5	0.9	0.9	0.77	0.35	1.6	3.45					1	4.2	0.07	4.2	0.07						
6	0.9	0.9	0.7	0.37	1.6	3.7	0.95	0.82	0.42		1	4.2	0.07	4.2	0.07	2.4	0.07	2.4	0.07	2.4	0.07
7	0.9	0.9	1.18	1.13	0.5	4.5				4.8	1	2.4	0.07	5.5	0.017						
8	0.9	0.9	0.82	1.2	0.6	3.9	0.95	0.95	1.3	4.1	1	4.2	0.07	2.4	0.07	5.5	0.017	5.5	0.017	4.2	0.07

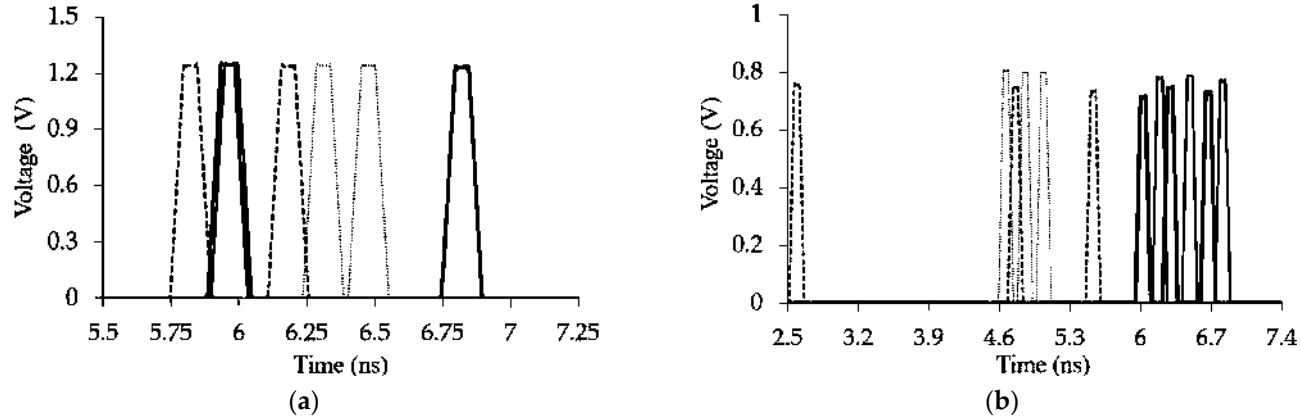

Figure 11. Voltage waveforms at the output of (**a**) MFs 1–4 and (**b**) MFs 5–8 in the lossless simulation, where MFs 1 and 5 (—), MFs 2 and 6 (—-), MFs 3 and 7 (···), and MFs 4 and 8 (- -).

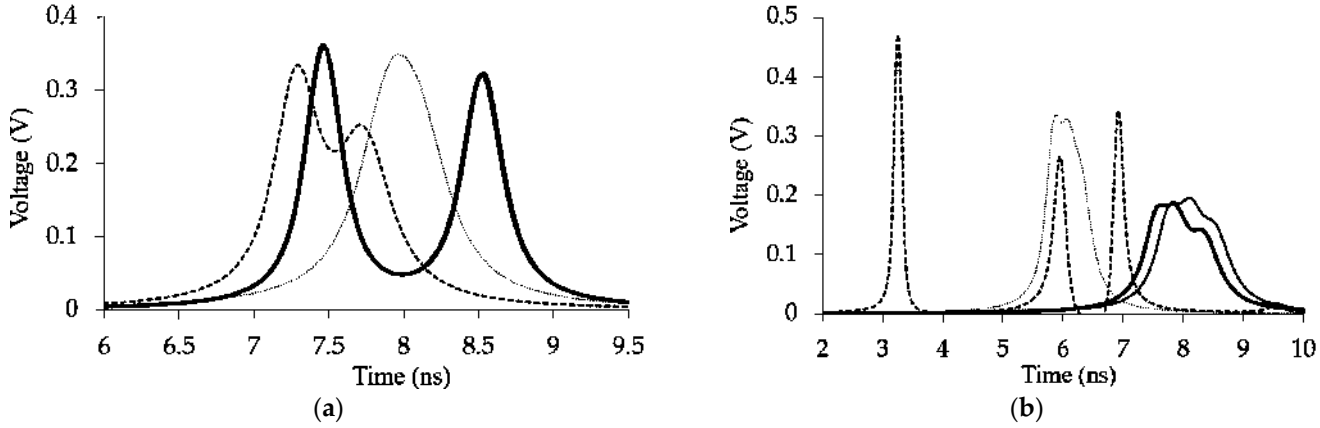

Figure 12. Voltage waveforms at the output of (**a**) MFs 1–4 and (**b**) MFs 5–8 in the lossy simulation, where MFs 1 and 5 (—), MFs 2 and 6 (—-), MFs 3 and 7 (···), and MFs 4 and 8 (- -).

Since there are only two conductors (in addition to the reference one) in MFs 1–4 located symmetrically, it was possible to achieve complete decomposition of the exciting UWB pulse without changing the arrangement of the conductors. However, the rest of the resources (changing the geometric and electrophysical parameters of the MF) were used for optimization. As can be seen from Figure 11a and Table 5, MFs 1 and 2 show equal values of maximum output voltage (1.25 V) and high $\Delta\tau$ values between DPs (0.85 ns/m). The CSs of MFs 1 and 3 were previously analyzed in [31,41], which is why the optimization with real parameters did not require much effort. However, in MF 3, since the reference conductor represents an external shield, it was not possible to obtain the high $\Delta\tau$ value (0.16 ns/m). This situation was improved by adding an external dielectric to the active and passive conductors (transition from MF 3 to MF 4). Thus, in MF 4, the $\Delta\tau$ value was already 0.35 ns/m. Meanwhile, in the lossless simulation, the maximum output voltage value for

MFs 3 and 4 is less (1.24 V) than in MFs 1 and 2 (1.25 V), which is two times less than the value of U_{in}. In addition, we can talk about an acceptable matching of MFs 1–4 with the path because the value of U_{in} is close to half the EMF, i.e., 2.5 V (maximum deviation for MF 2 is 2.7%). Thus, when simulating MFs 1–4 without losses, it is possible to increase the exciting pulse duration to 0.846 ns for MFs 1 and 2, to 0.156 ns for MF 3, and to 0.34 ns for MF 4 with the same attenuation coefficient.

Table 5. Simulation results for MFs 1–8 in the lossless simulation.

MF	U_{in}, V	DP Amplitudes U_i, V			Differences in Per-Unit-Length Delays $\Delta\tau_i$, ns/m	
		U_1	U_2	U_3	$\Delta\tau_1$	$\Delta\tau_2$
1	2.56	1.25	1.24		0.85	
2	2.64	1.25	1.23		0.85	
3	2.48	1.24	1.24		0.16	
4	2.48	1.24	1.24		0.35	
5	2.38	0.77	0.78	0.78	0.3	0.33
6	2.37	0.71	0.74	0.73	0.27	0.37
7	2.24	0.8	0.8	0.8	0.19	0.18
8	2.45	0.75	0.75	0.73	2.18	0.77

Table 6. Simulation results for MFs 1–8 in the lossy simulation.

MF	U_{in}, V	Decomposition Pulses Amplitudes U_i, V			Differences in Per-Unit-Length Delays $\Delta\tau_i$, ns/m	
		U_1	U_2	U_3	$\Delta\tau_1$	$\Delta\tau_2$
1	2.55	0.36	0.32		0.85	
2	2.6	0.36	0.32		0.85	
3	1.84	0.35	0.35		0.16	
4	1.92	0.33	0.25		0.35	
5	2.35	0.18	0.19	0.17	0.3	0.33
6	2.34	0.16	0.19	0.14	0.27	0.37
7	2.22	0.33	0.33	0.3	0.19	0.18
8	2.42	0.47	0.26	0.34	2.18	0.77

Because conductor 3 is in MFs 5–8, it is important to ensure different couplings between the conductors during optimization. This is possible by changing their arrangement, as well as the geometric and electrophysical parameters of the passive conductors, and internal and external insulation. As follows from Table 6, the use of conductor 3 allowed for the increase in the overall MF attenuation. Thus, among MFs 5–8, the maximum attenuation of the exciting UWB pulse is observed in MF 6 (0.74 V), which is 3.2 times less than the U_{in} value. The maximum amplitude is observed for MF 7 (0.8 V), which is 2.8 times less than the U_{in} value. As can be seen from Figure 11b and Table 6, MF 5 provides an output voltage level of 0.78 V. However, by adding an external dielectric to the active and passive conductors (transformation of MF 5 into MF 6), it was possible to reduce the maximum output voltage level to 0.74 V. Nevertheless, the $\Delta\tau_i$ values decreased from 0.3 and 0.33 ns/m to 0.27 and 0.37 ns/n. When MF 7 was transformed into MF 8 by adding an external dielectric to the active and passive conductors, it was also possible not only to reduce the level of the maximum output voltage from 0.8 V to 0.75 V but to increase the values of $\Delta\tau_i$ from 0.19 and 0.18 ns/m to 2.18 and 0.77 ns/m. The matching of MFs 5–8 with the path is also acceptable (the maximum deviation for MF 7 is 5.5%). Thus, in lossless simulations of MFs 5–8, it was possible to increase the exciting pulse duration to 0.291 ns for MF 5, to 0.261 ns for MF 6, to 0.186 ns for MF 7, and to 0.76 ns for MF 8 with the same attenuation coefficient.

Figure 12a,b show the output voltage waveforms from the MFs 1–8 simulations that considered losses. It is important to note that the optimization of MFs 1–8 was performed for the lossless case. In view of this, on the obtained time responses, the achievability

of the optimization criteria (equalized amplitudes of DPs, aligned and maximized time intervals between DPs) is weakly observed. However, Figure 12a and Table 6 illustrate the complete coincidence of the output voltage waveforms, as well as the U_i and $\Delta\tau$ values for MFs 1 and 2. At the same time, due to the high $\Delta\tau$ value, in comparison with other MFs, this configuration (with this representation of the central reference conductor) is more preferable for implementing 2-conductor MFs with a circular CS (even with a higher maximum output voltage value compared to MFs 3 and 4). In the case of MF 3, one can see the complete superposition of DPs due to dispersion and the low $\Delta\tau$ value (0.16 ns/m). MF 4 also has a low $\Delta\tau$ value (0.35 ns/m), which results in a partial superposition of DPs. From Figure 12b and Table 6, it can be seen that the $\Delta\tau_i$ values for MFs 5 (0.3 and 0.33 ns/m) and 6 (0.27 and 0.37 ns/m) are not enough for complete decomposition of the exciting UWB pulse in the lossy simulations. Despite the obvious superposition of mode pulses, these MFs provide the lowest value of the maximum output voltage (0.19 V) among all 3-conductor MFs with a circular CS. This is probably caused by the influence of losses in the MFs because the matching of the MFs with the path remains acceptable (deviation from U_{in} is 3%). The output voltage waveforms of MFs 7 and 4 are similar: there is a partial superposition of DPs because of the low $\Delta\tau_i$ value (0.19 and 0.18 ns/m). Finally, at the output of MF 8, complete decomposition of the exciting UWB pulse is observed because of high $\Delta\tau_i$ values (2.18 and 0.77 ns/m). However, the output voltage amplitude level of MF 8 is the highest among all 3-conductor MFs (0.47 V). Nevertheless, based on the data obtained, this MF is the most promising for experimental study.

5. Experimental Studies of Modal Filters with a Circular Cross-Section

Prototypes of MFs with a circular cross-section were developed and created in three types: circular 3-conductor cable, flat 3-conductor cable, and circular 4-conductor cable. In addition, we present the results of a comparative analysis of the calculated and measured MF characteristics. CSs and equivalent circuits of prototypes with the length l = 2 m are presented in Figure 13. The CS parameters of the considered MF are presented in Table 7.

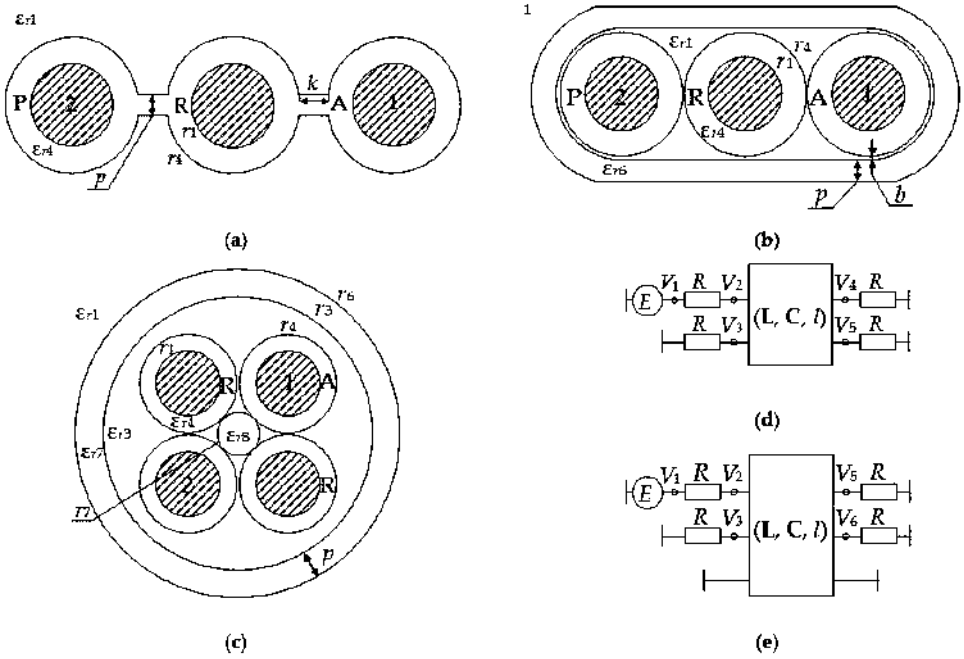

Figure 13. CSs of (**a**) MF 1, (**b**) MF 2, (**c**) MF 3, and (**d**,**e**) equivalent circuits of real MF configurations with a circular CS.

Table 7. The parameters of MF 1–3 prototypes (*k* and *p*—the length and thickness of separation base (insulation), *b*—the distance between internal and external insulations).

MF	r_i, *k*, *p*, *b*, mm								ε_{ri} and $tg\delta_i$									R, Ω	The Dimensions, mm
	r_1	r_3	r_4	r_6	r_7	*k*	*p*	*b*	ε_{r1}	ε_{r4}	$tg\delta_4$	ε_{r6}	$tg\delta_6$	ε_{r7}	$tg\delta_7$	ε_{r8}	$tg\delta_8$		
1	1.3		2.07			0.9	0.6		1	3.4	0.05							116	14 × 4.2
2	1.4		2.4				0.95	0.15	1	3.0	0.02	3.5	0.05					87	16.6 × 6.9
3	1.88	7.75	2.82	9.31	1.22		1.5		1	2.8	0.01	3.4	0.02	4.6	0.05	4.6	0.06	43.33	18.62 × 18.62

MF 3 is a symmetrical 4-conductor structure, so the complete decomposition of the exciting UWB pulse in it is impossible. Therefore, during the measurements, two of the four conductors were assumed to be references, but this case can be simulated in two ways: by setting the second reference conductor to an ideal «ground» (Figure 13d) or by setting it to signal and shorted to ground (Figure 13e). The geometric mean resistance for the first case is 43.33 Ω. In addition, MF 1 was simulated in the electrodynamic simulation system. Figure 14 shows the appearance of a geometric model with a printed circuit board (PCB) at one end (in the simulation, at both ends).

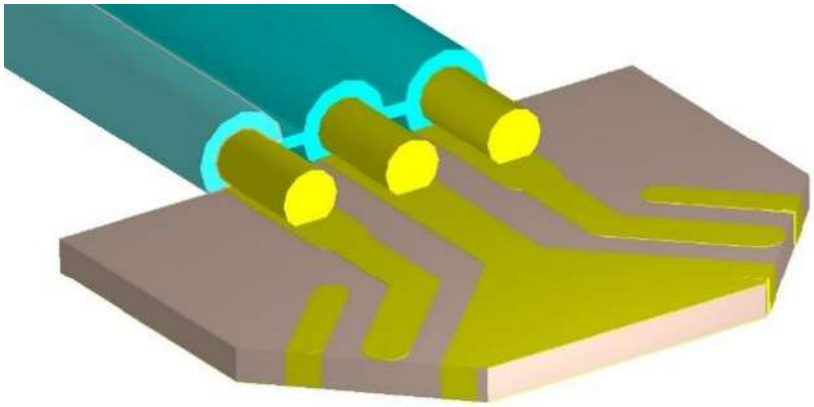

Figure 14. Geometric model of MF 1 with a PCB.

As an excitation, we used a pulse signal that was received as a result of taking the derivative of a real step excitation obtained using a Tektronix DSA 8300 oscilloscope, with an EMF amplitude of 0.634 V, a rise time of 14.6 ps, a fall of 12 ps, and a flat top of 4.7 ps (at levels 0.1–0.9), and the total duration (at level 0.5) is 22 ps. Figure 15 shows the waveforms of the step excitation and the signal derived from it, as well as voltage spectral density and the measurement setup with the Tektronix DSA 8300 oscilloscope.

Figure 16 shows MF prototypes with a circular CS. To surface mount the SMA connectors, we made PCBs that are connected to the MF at the ends (Figure 17). In MFs 1 and 2, the central conductor is taken as a reference. In MF 3, when measuring, two diagonal (in terms of CS) conductors were taken as reference. The SMA connectors were installed at the ends of all conductors to connect the MF to the measuring path. During measurements, *R* values with a resistance of 50 Ω were installed on the SMA connectors of the passive conductors.

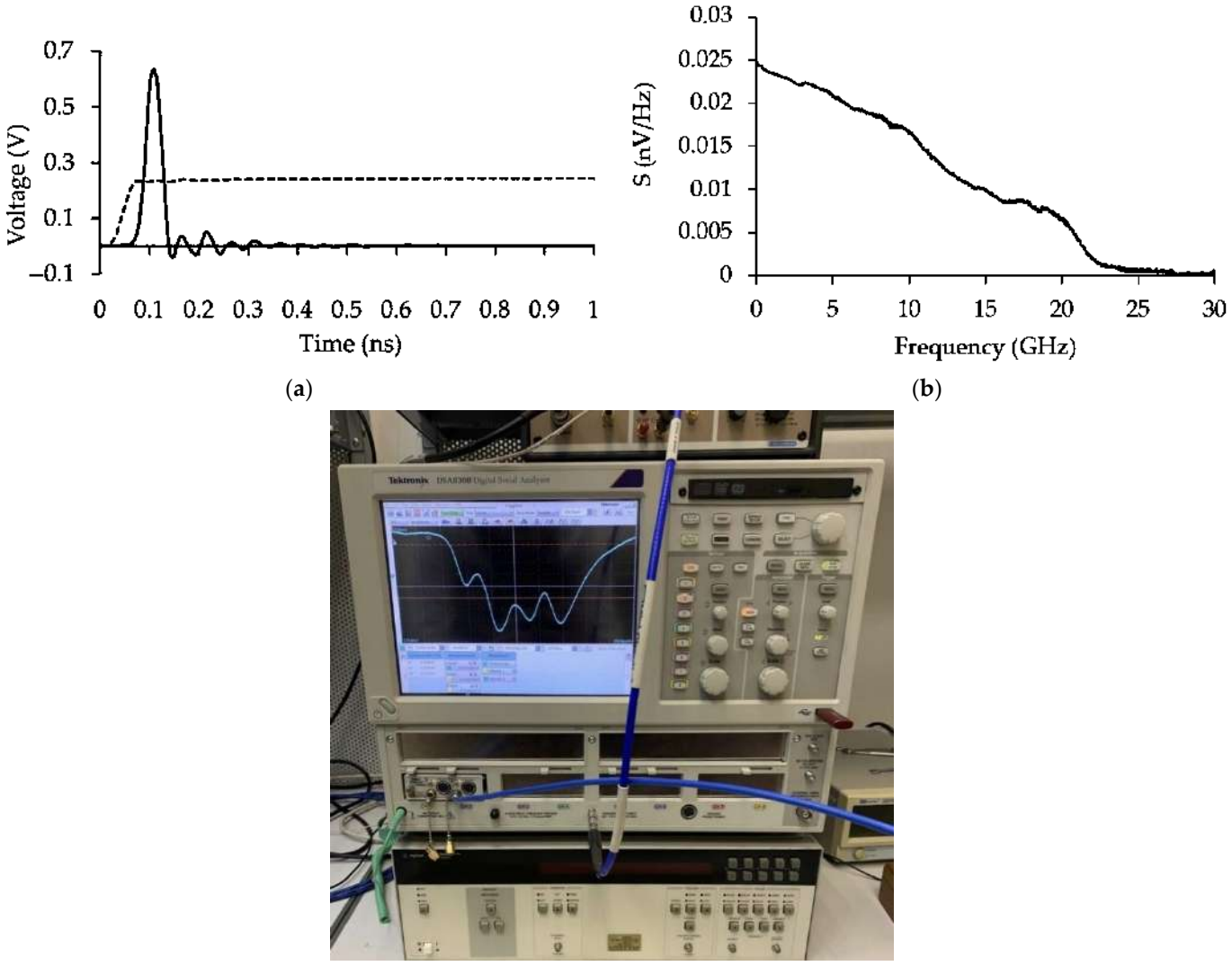

Figure 15. Waveforms of (**a**) step excitation (- -) and a derived real UWB pulse (—-) with time shift, its (**b**) voltage spectral density, and (**c**) the measurement setup with the Tektronix DSA 8300 oscilloscope.

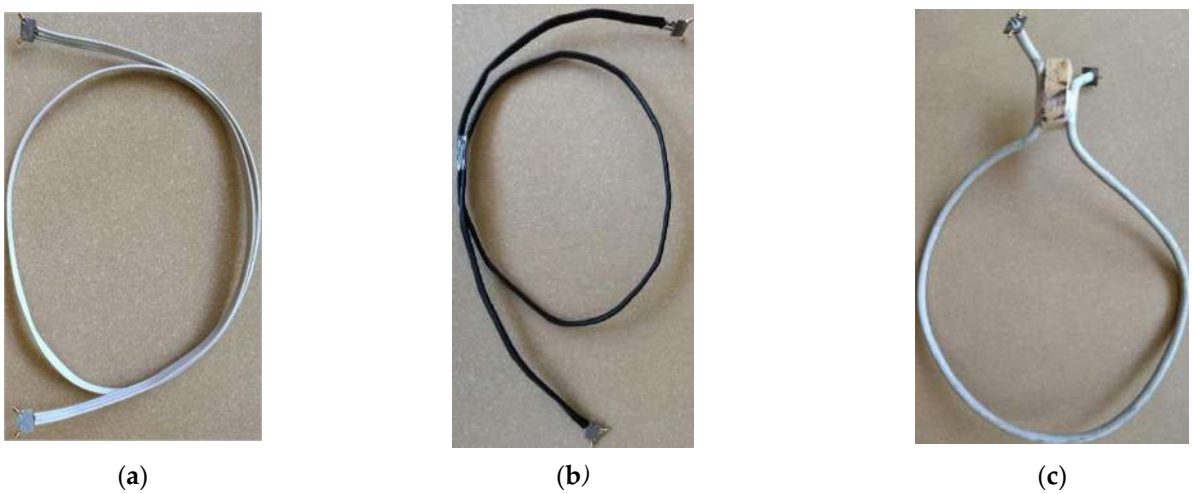

Figure 16. Prototypes of (**a**) MF 1, (**b**) MF 2, and (**c**) MF 3.

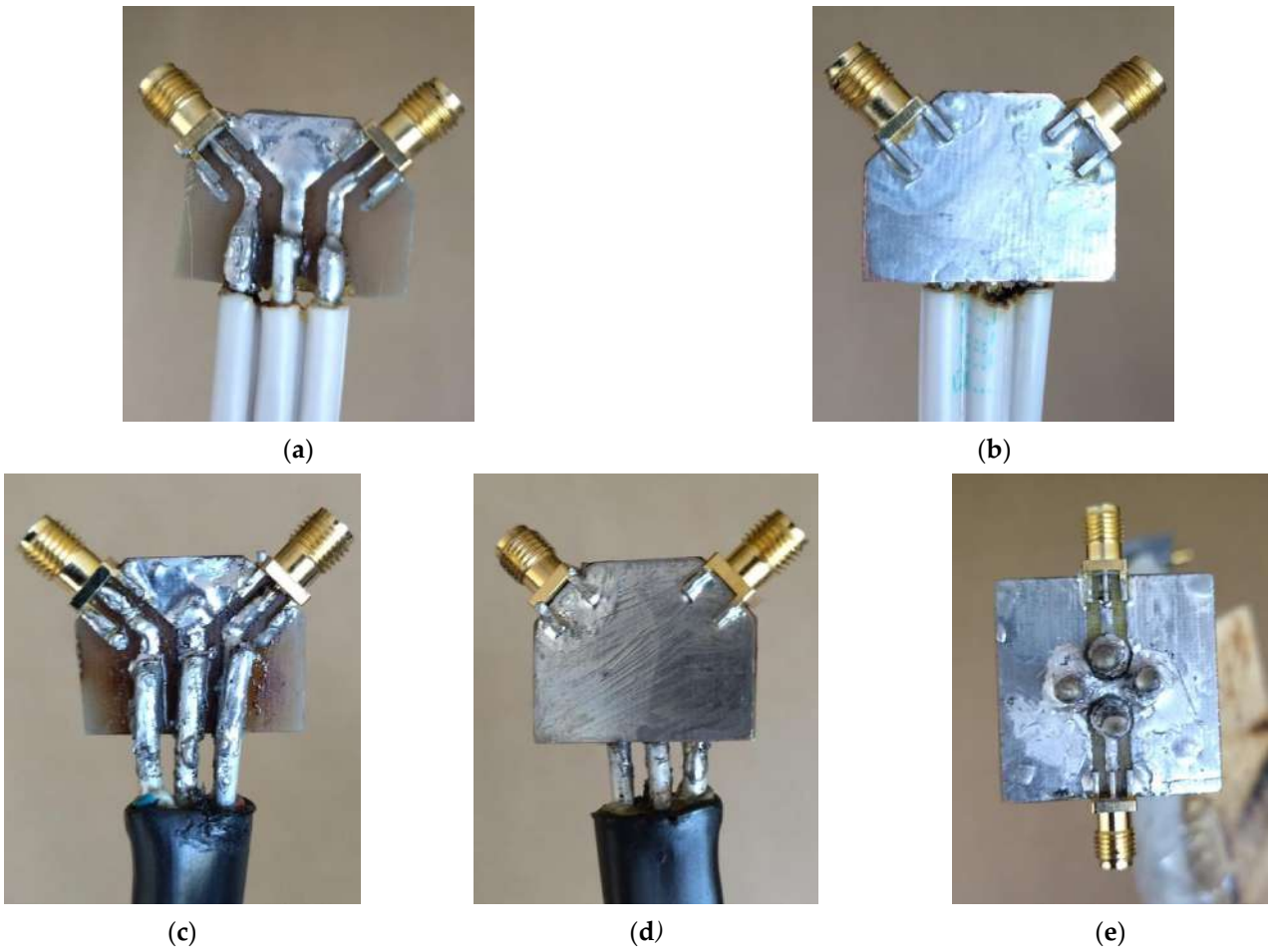

Figure 17. PCBs surface-mounted on (**a**,**b**) MF 1, (**c**,**d**) MF 2, and (**e**) MF 3.

The characteristics of MFs 1–3 in the time and frequency domains are presented below. Figure 18 shows the measurement setup with the Panorama P4226 vector electrical circuit analyzer and the frequency dependences of $|S_{21}|$ for each of the prototypes that were measured using it.

The measurement results demonstrate that the bandwidth of MFs 1–3 is 0.19–0.41 GHz. For MF 1 at a frequency of 3.8 GHz and for MF 2 at 2.8 GHz, the minimums are observed at minus 40 dB, and for MF 3, at minus 32 dB at a frequency of 1.7 GHz.

Figure 19 shows the voltage waveforms at the output of MFs 1–3, which were obtained in lossy simulations and experimentally (there is a coincidence of the voltage waveforms obtained for various reference conductors from Figure 13d,e). The simulation of MF 3 was also performed using the equivalent circuit from Figure 13e to compare two types of simulation of a 4-conductor MF with two reference conductors. The maximum output voltage values were 0.029, 0.023, and 0.03 V during measurements and 0.024, 0.014, and 0.022 V during simulation for MFs 1–3. The maximum deviation of the obtained values during measurements and simulation was 39% for MF 2. The measurements showed that the values of the maximum output voltage were 21.8, 27.5, and 21.1 times less than the EMF amplitude for MFs 1–3. The maximum output voltage in MF 1 during the electrodynamic simulation was 0.017 V, which is 37 times less than the EMF.

(**a**)

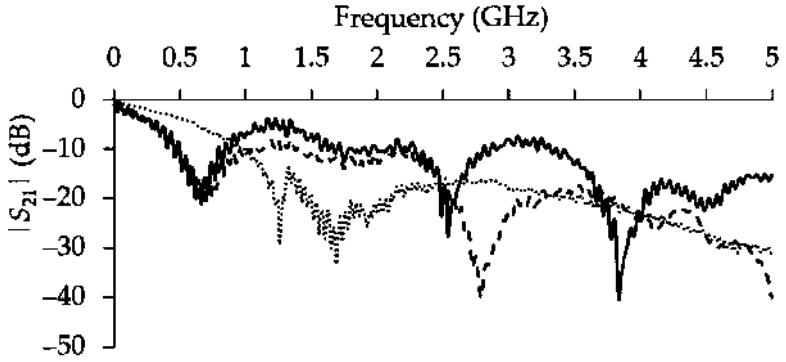

(**b**)

Figure 18. (**a**) The measurement setup with the Panorama P4226 vector electrical circuit analyzer and (**b**) frequency dependences of $|S_{21}|$ for MF 1 (—-), MF 2 (- -), and MF 3 (· ·).

It can be seen that the output signal arrives at approximately the same time. Unfortunately, due to the dispersion, it is impossible to accurately determine the arrival time of each pulse during measurements. In addition to dispersion, the voltage waveforms obtained by simulation are also affected by losses in conductors and dielectrics. This leads to an increase in the rise and fall times of each output pulse and to their partial overlap. This is especially clearly observed for MF 3. In general, there is a consistency in the output voltage waveforms, which is obtained experimentally and through simulation.

Note the presence of a third pulse in the measurements of MFs 1 and 2. Since the interval between the peaks of pulses 2 and 3 in the measurements is approximately 0.3 ns for both MFs, the pulses may appear because of the boundary conditions of the MF and the PCBs that are connected to them (because the dielectric filling in the CS of MF 2 is different from MF 1). The PCBs are designed to connect with SMA connectors in a 50 Ω path, while the geometric mean resistances of MFs 1 and 2 are 115 and 87 Ω. This causes a mismatch and the appearance of reflections in the measured path. To verify this statement, MF 1 was simulated, taking into account the PCBs at the ends (Figure 20).

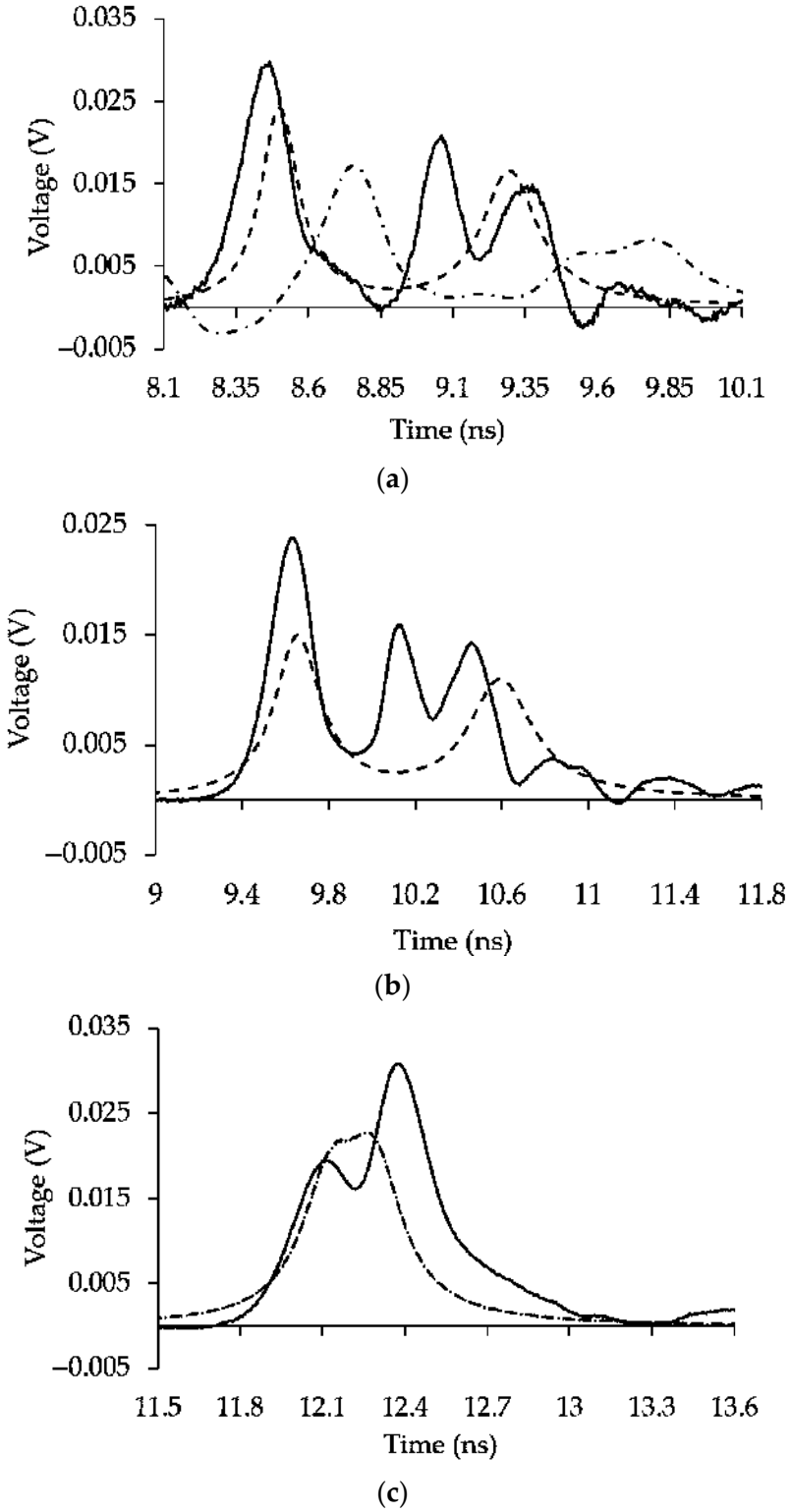

Figure 19. Voltage waveforms at the output of (**a**) MF 1, (**b**) MF 2, and (**c**) MF 3, obtained by lossy simulation (– –) (including MF 1 in the electrodynamic simulation system (- · -) and MF 3 by the equivalent circuit from Figure 13e (· ·)) and experimentally (—-).

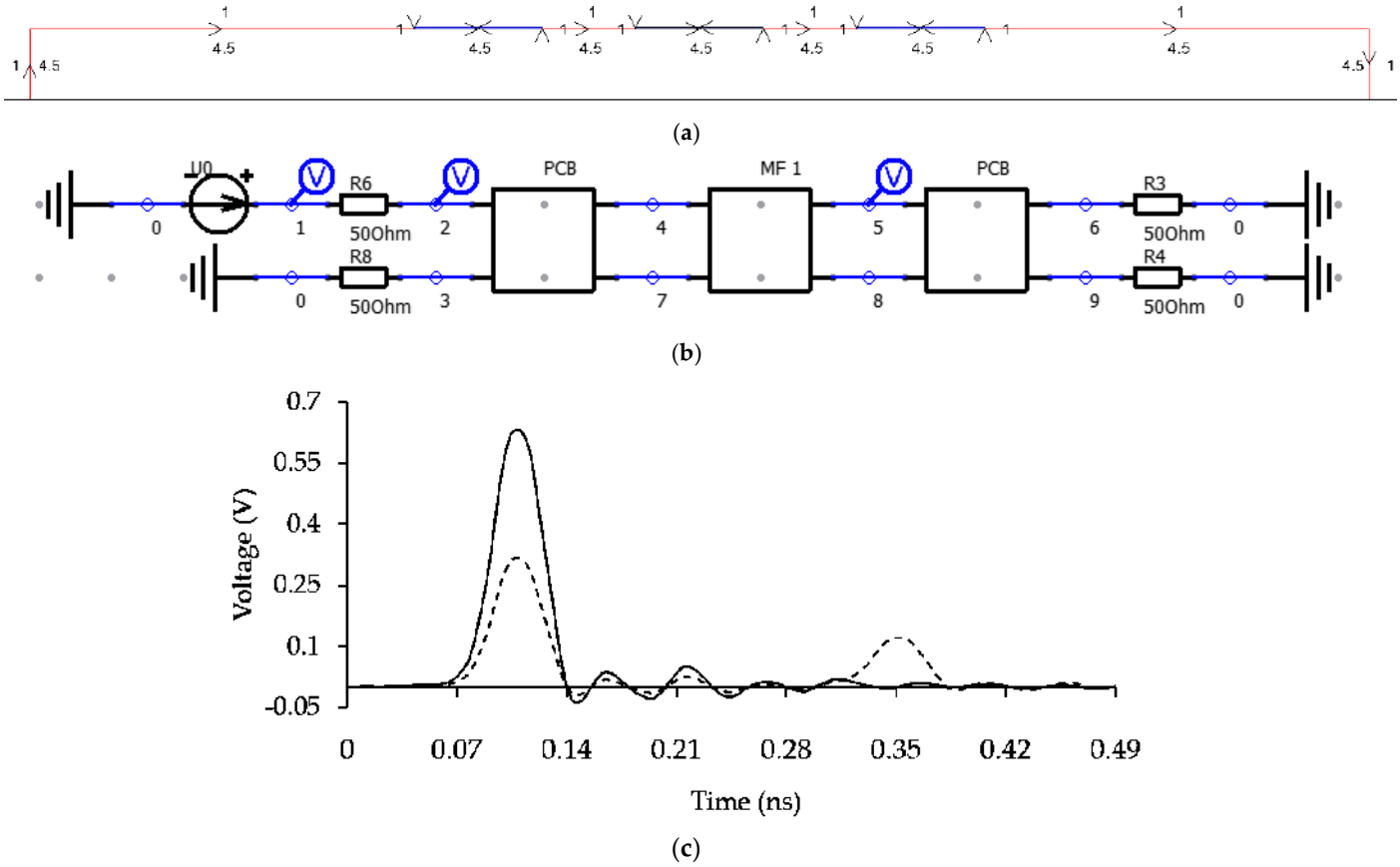

Figure 20. (**a**) CS of PCBs at the ends of the MF, (**b**) connection diagram of MF 1 with PCBs at the ends, as well as waveforms of (**c**) EMF (—-) and voltage at the input (- -) of the PCB during simulation.

It can be seen that not one but two pulses are observed at the PCB input, the second being half the first in amplitude. This is confirmed by the measurement results from Figure 19a, where pulse 3 is clearly visible, which is the result of reflections caused by the mismatch. Finally, the presence of pulse 3 is also confirmed by the electrodynamic simulation in Figure 19a, where the superposition of pulses 2 and 3 is observed. Meanwhile, there is a shift of all waveforms of the output voltage over time. It can be caused by the difference in relative dielectric permittivities.

6. Optimization of Modal Filters by Evolutionary Strategies

6.1. Optimization Features for Modal Filters with a Circular Cross-Section and Strip Modal Filters

As noted earlier, MFs are traditionally implemented in the form of strip structures; however, both for MFs with a circular CS and for strip MFs, the optimization is always important. To begin with, the optimization approaches for both types of MFs will have some similarities. For example, parametric optimization equally implies the search for such a set of optimal parameters of the structure, in which the developed MF will best answer the purpose. However, there are more differences in optimization features because of the significant differences in configurations.

The first and most significant difference in the optimization of strip MFs and MFs with a circular CS is the peculiarity of their creation in the TALGAT system. When optimizing strip structures, the optimized parameters change and do not allow overlapping of CS elements. The construction of CS elements usually starts from zero, and each subsequent «Line» object is not only related to the previous one but can also have its own mutable variable, as seen in Figure 21a. In the TALGAT system, the «Line» object is a segment that requires the setting of the initial and final coordinates (x; y). However, when constructing structures with a circular CS (Figure 21b), we use the «Circle» object (circumference that

requires specifying the coordinates (x; y) of its center as well as the radius, as seen in Figure 21b). In this case, the symmetry of conductors will lead to the coincidence of the arrival times of certain modes. This problem is solved by changing the coupling of the active conductor with the passive one by breaking the symmetry in the conductor's arrangement. Therefore, it is necessary to set random coordinates (x; y), which leads to the problem when the conductors go out of acceptable boundaries and overlap with other objects. This happens because the coordinates of individual conductors are not related to each other. Therefore, the optimization of the MF with a circular CS was performed exclusively manually, using the HS_{opt}.

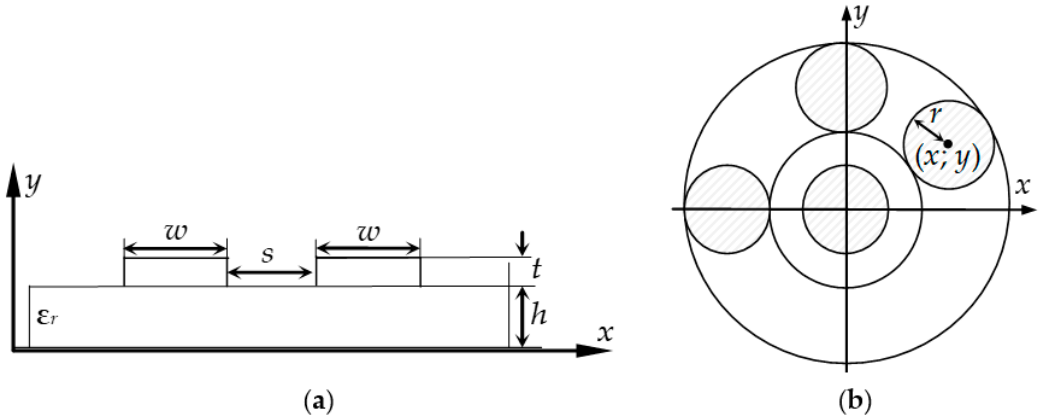

Figure 21. Creating the CS of the MF (**a**) based on an MSL and (**b**) with a circular section.

The second difference follows from the first, in particular, the use of different coordinate systems. We use the Cartesian coordinate system when constructing the CS of stripe structures and optimizing them. The Cartesian coordinate system is ideal for such structures. However, for optimizing an MF with a circular section, the polar coordinate system is a more convenient option because, in this system, the coordinates of a point are determined by the angle and radius.

The third difference is expressed in the floating boundary conditions, which, in this case, means the range of the optimized parameters. As is known, when optimizing strip MFs we can set the boundary conditions with exact values based on the given requirements and physical feasibility. In this case, as noted earlier, there is no risk of superposition of conductors and dielectrics. In an MF with a circular CS, it is possible to set exact values only for the values of the radius of the elements and only on the condition that the distance from the center of the conductor to the origin of coordinates is fixed. However, as the radius of the elements changes, their boundaries may be located closer to or further from the center of coordinates, which increases the risk of overlapping neighboring elements. Among other things, the main difficulty lies in finding the position of the conductors relative to each other because, in this case, we cannot accurately indicate the boundary conditions of the parameters to be optimized (because they are unknown to us). Based on this, when we optimize the MF with a circular CS, it is recommended to use variables as boundary conditions for the angle where the conductor center is located. These variables, in turn, depend on other parameters that change during the optimization process (for example, the radius of the conductors, and the distances from the center of the conductors to the coordinate origin).

The fourth difference is the methods that are used to optimize the MF. Strip MFs are usually optimized using GA and ES. These evolutionary algorithms cope perfectly with their task and, at the same time, show high efficiency. However, due to the peculiarities of constructing MFs with a circular CS in the TALGAT system, which were mentioned above, their optimization is performed by the HS_{opt}. Among other things, multicriteria optimization is currently implemented only with the help of GA.

Thus, the main feature differentiating optimization of an MF with a circular CS and a strip MF is that they are constructed differently in the computer simulation system. Obviously, the optimization using evolutionary algorithms is not suitable for MFs with a circular CS. Nevertheless, we can create a new technique for solving this problem.

6.2. Novel Optimization Technique for Modal Filters with a Circular Cross-Section

As noted earlier, the main problem in optimizing an MF with a circular CS is the risk that conductors will overlap with each other or on the dielectric boundaries. This can happen when there is a search for the optimal position of the conductors within the structure or the size of these conductors increases. The solution to this problem is to change from the Cartesian coordinate system to the polar one. This way, the position of the conductor in space will be determined not by two coordinates (x; y) but by the radius (distance R from the center of the conductor to the zero point) and the angle φ relative to the horizontal axis (x) as well (see Figure 22).

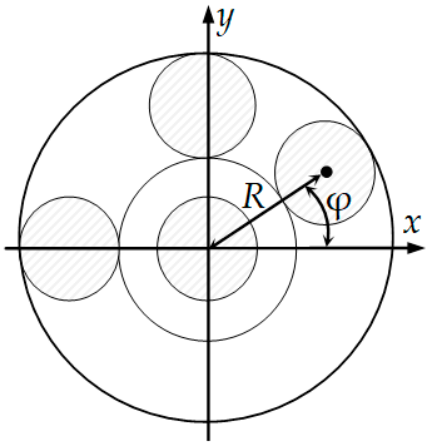

Figure 22. Determining the position of the conductor according to the polar coordinate system.

To keep the CS correct, we took the angles (in degrees) as the boundary conditions. The minimum angle between the centers of the active and each of the passive conductors was determined by

$$\alpha = \frac{180(\sum r_{Ci})}{\pi R_{\mathrm{PA}}}, \tag{4}$$

where R_{PA} is the distance from the zero point to the center of the passive and active conductors. For simplicity, this value is taken the same for passive and active conductors and equal to the value for passive ones. The r_{Ci} is the radius of adjacent conductors, between which the angle should be found.

Assuming the active conductor location angle α_{A} to be constant, the boundary conditions for each optimized (relative to active) conductor using (4) will look like

$$\varphi = \alpha_{\mathrm{A}} \pm (\alpha + 3), \tag{5}$$

where for the second (according to the order) conductor (which is the first passive conductor), which is exemplified in Figure 4a, the boundary will be determined by subtracting the obtained angle α from the fixed α_{A}. In addition, the addition of another 3° to the angle α will prevent the conductors from contacting. In this case, for the third (according to the order) conductor (which is the second passive conductor), the boundary will be determined by the sum of these angles. Note that the proposed method for optimizing an MF with a circular CS is suitable for an MF with any number of conductors.

6.3. Optimization of a 3-Conductor Modal Filter with a Circular Cross-Section

To begin with, we decided to optimize the MF with only two parameters, φ_1 and φ_2, to test the methodology proposed in Section 6.2. The optimization was performed using a modified ES algorithm that allows setting the ranges of the parameters to be optimized [40]. This method is implemented in Python with the ES algorithm library included. This aspect allows using variables as boundary conditions. Without this feature, appropriate optimization of the cable MF will be impossible because in this MF, the boundaries for determining the optimal parameters depend on the parameters being changed. As such, we cannot use GA optimization since this algorithm is implemented directly in the TALGAT system in the built-in language and takes only numbers as arguments that are responsible for the boundaries for finding the optimal value.

To test the technique, we chose a 3-conductor MF from Figure 4a. The fixed values of the CS parameters are chosen as follows: $\varepsilon_{r1} = 1$, $\varepsilon_{r2} = 5$, $\varepsilon_{r3} = 19$, $r_{\mathrm{R}} = 0.9$ mm, $r_{\mathrm{A}} = 0.9$ mm, $r_{\mathrm{P1}} = 0.9$ mm, $r_{\mathrm{P2}} = 0.89$ mm, $r_{\mathrm{td}} = 0.7$ mm, $R_{\mathrm{P1}} = 2.525$ mm, $R_{\mathrm{P2}} = 2.525$ mm. In this work, losses were not taken into account in order to exclude their influence at this stage of the study. As an excitation, we used a trapezoidal UWB pulse with an EMF of 5 V, a flat top duration $t_{\mathrm{d}} = 50$ ps, and a rise and fall time $t_{\mathrm{r}} = t_{\mathrm{f}} = 50$ ps (the total duration of the UWB pulse was $t_{\Sigma} = 150$ ps). The length of the MF was equal to 1 m. The load values were equal to 50 Ω. As input parameters (initial solutions) for the algorithm, the list of starting points was used for each optimization parameter and an initial step size that is adapted and modified during the optimization process. The ranges for angle optimization were the following: φ_1 from 10° to the boundary, which is determined by formula (5); φ_2 from the boundary, which is determined by formula (5) to 350°. The initial solutions for ES optimization were as follows: $\varphi_1 = 45°$, $\varphi_2 = 260°$, and the step is $\sigma = 5°$.

Table S5 (in Supplementary Materials) shows the optimization results for a 3-conductor MF with a circular CS by ES with limitations. In Table S5, N is the number of runs, and N_{it} is the number of calculations at one run. Optimization was performed according to the amplitude criterion (minimization of the maximum output voltage value (U_{max})). Table S5 summarizes the values of the optimized parameters, U_{max}, as well as the calculation time and stopping criteria (SC) during ES operation. During optimization, the following ES SC were obtained: I is the stop when the number of calculations reached its maximum, P is when the values of the optimized parameters converged, and Q is the stop when the objective function converged. Figure 23 shows the CS of a circular MF after 2-parameter optimization and the best-case MF output voltage waveforms.

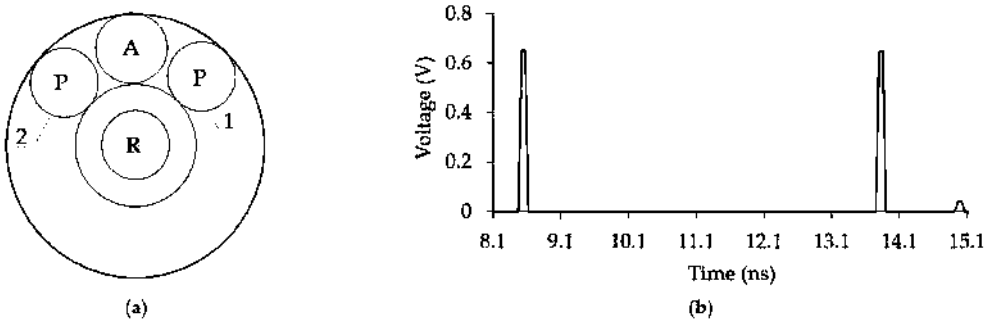

Figure 23. (**a**) CS and (**b**) output voltage waveform of a 3-conductor MF with a circular CS after 2-parameter optimization.

From Table S5 and Figure 23, we can see that the smallest value of the voltage at the MF output is 0.652 V (at 5000 calculations). The voltage value at the MF input, in this case, was 1.58 V, and the minimization of U_{max} was achieved by equalizing the amplitudes of modes 1 and 2. The τ_i values with the parameters after optimization were 8.47, 12.85, and 13.75 ns/m, and the $\Delta\tau_i$ values were 4.38 and 0.9 ns/m. Note that to find a solution, the algorithm requires 2000–5000 calculations and 2000–7000 s per run. Meanwhile, even with two optimized parameters, the minimum U_{max} value was 0.652 V.

6.4. Optimization of a 4-Conductor Modal Filter with a Circular Cross-Section by Evolutionary Strategies with Limitations

When optimizing a 4-conductor MF with a circular CS (Figure 6c), the following conditions were applied: active and reference conductors are fixed; radius values of passive conductors (r_{P1}, r_{P2}, r_{P3}), distances from the center of passive conductors to the origin (R_{P1}, R_{P2}, R_{P3}), angles (φ_1, φ_2, φ_3) between the x-axis and these centers and internal dielectric thickness (r_{td}) are optimized. Figure 24 visualizes these conditions, where r_{d1} is the radius of the internal dielectric relative to the origin, and r_{d2} is the radius of the external dielectric relative to the origin.

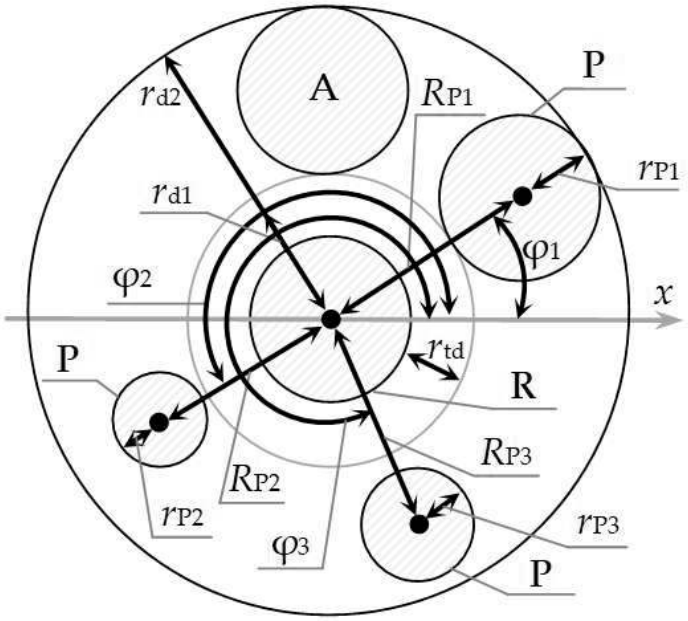

Figure 24. Optimized parameters for a 4-conductor MF with a circular CS.

The fixed values of the CS parameters are chosen as follows: $\varepsilon_{r1} = 1$, $\varepsilon_{r2} = 2.4$, $\varepsilon_{r3} = 4.2$, $r_R = 0.9$ mm, $r_A = 0.9$ mm. The excitation parameters, as well as the lengths and loads at the ends of the MF, were taken the same as in Section 6.3.

Table S6 (in Supplementary Materials) shows the results of the optimization performed according to the amplitude criterion. Table S6 summarizes the values of the optimized parameters (φ_1, φ_2, φ_3 in degrees, the rest in mm), U_{max} in volts, calculation time in seconds, and stopping criteria during ES operation. The boundary conditions for the optimized parameters are the following: r_{P1}, r_{P2}, and r_{P3} from 0.5 to 0.9 mm, r_{td} from 0.1 to 0.7 mm, R_{P1}, R_{P2}, and R_{P3} from the difference ($r_{d2} - r_{P1/P2/P3} - 25$ µm) to the sum ($r_{d1} + r_{P1/P2/P3} + 25$ µm), φ_1 from 10° to the boundary, which is determined by formula (5), φ_2 from the boundary, which is determined by formula (5) to 260°, for φ_3 both boundary conditions are determined by formula (5). I=The initial solutions are the following: r_{P1}= 0.7 mm, r_{P2}= 0.7 mm, r_{P3}= 0.7 mm, r_{td}= 0.5 mm, R_{P1}= 2.45 mm, R_{P2}= 2.45 mm, R_{P3}= 2.45 mm, φ_1= 45°, φ_2= 260°, φ_3= 315°, and the step is σ = 0.1 mm. Figure 25 shows the output voltage waveforms of a circular 4-conductor MF, as well as its CS after 10-parameter optimization for identifying the best result.

Table S6 and Figure 25 illustrate that the minimum U_{max} value is 0.53 V (with 500 calculations). As we know, when matching with the path, the U_{in} value is equal to half the EMF of the source. After ES optimization, the U_{in} level was 1.83 V (whereas in the matched case, it would tend to 2.5 V). The τ_i values were 5.49, 5.71, 6.11, and 6.56 ns/m, and $\Delta\tau_i$ were 0.22, 0.4, and 0.45 ns/m. In all cases, the algorithm stopped calculations when the specified number of iterations came to an end. With 5000 calculations, the algorithm needed about 17,570 s per run, but the best result was obtained with fewer iterations (500

in this case). This could be explained by the use of randomness in the algorithm of the modified ES.

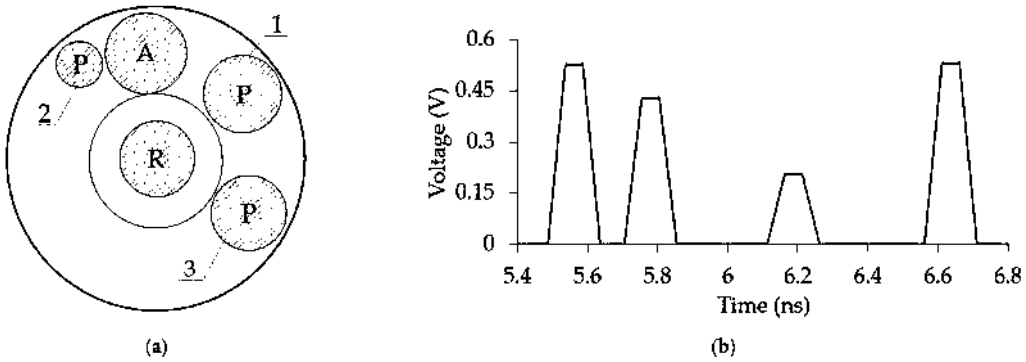

Figure 25. (**a**) CS and (**b**) output voltage waveform of a 4-conductor MF with a circular CS after 10-parameter optimization.

6.5. Optimization of a 3-Conductor Modal Filter with a Circular Cross-Section with Insulation around the Conductors by Evolutionary Strategies with Limitations

When a 3-conductor MF with a circular CS with insulation around the conductors (Figure 10f) was optimized, the following conditions were applied: active and reference conductors were fixed; the values of r_{P1}, r_{P2}, R_{P1}, R_{P2}, φ_1, φ_2, dielectric thickness around the reference (r_{tdR}), active (r_{tdA}) and passive conductors (r_{tdP1} and r_{tdP2}) were optimized. Figure 26 visualizes these conditions, where r_{d1} is the radius of the internal dielectric relative to the origin, and r_{d2} is the radius of the external dielectric relative to the origin.

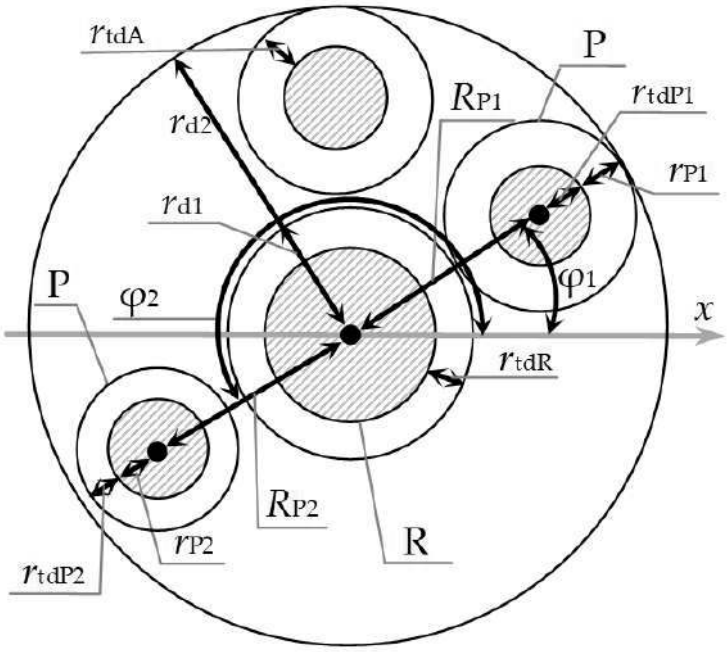

Figure 26. Variable parameters of a 3-conductor MF with a circular CS with insulation around the conductors.

Table S7 (in Supplementary Materials) summarizes the values of the optimized parameters, U_{max}, calculation time, and SC. The fixed values of the CS parameters are the following: $\varepsilon_{r1} = 1$, $\varepsilon_{r2} = 2.4$, $\varepsilon_{r3} = 4.2$, $r_R = 0.9$ mm, $r_A = 0.9$ mm. The excitation parameters, as well as the lengths and loads at the ends of the MF, were taken the same as in Section 6.3.

The boundary conditions for the optimized parameters are as follows: r_{P1} and r_{P2} from 0.5 to 0.9 mm, r_{tdR} from 0.1 to 0.7 mm, r_{tdA}, r_{tdP1}, and r_{tdP2} from 0.1 to 1 mm, R_{P1}

and R_{P2} from the difference ($r_{d2} - r_{P1/P2} - r_{tdP1/P2}$ + 25 μm) up to the sum ($r_{d1} + r_{P1/P2}$ + $r_{tdP1/P2}$ + 25 μm), φ_1 from 10° to the boundary, which is determined by formula (5), φ_2 from the boundary, which is determined by formula (5) up to 350°. Initial solutions are the following: r_{P1}= 0.7 mm, r_{P2}= 0.7 mm, r_{tdA}= 0.5 mm, r_{tdP1}= 0.5 mm, r_{tdP2}= 0.5 mm, r_{tdR}= 0.5 mm, R_{P1}= 2.45 mm, R_{P2}= 2.45 mm, φ_1= 45°, φ_2= 260°, and the step is σ = 0.1 mm. Figure 27 shows the output voltage waveforms of the MF under consideration, as well as its CS after 10-parameter optimization for the best result.

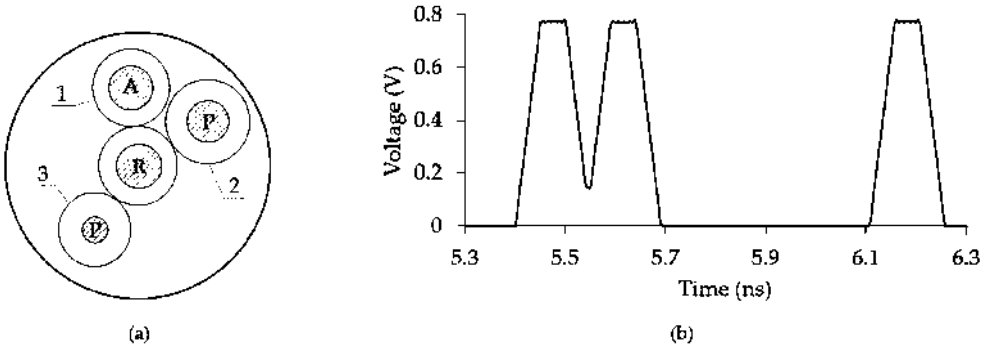

Figure 27. (**a**) CS and (**b**) output voltage waveform of a 3-conductor MF with a circular CS with insulation around the conductors after 10-parameter optimization.

From Table S7, it can be seen that the minimum U_{max} value is 0.78 V (with 5000 calculations). At the same time, Table S7 shows the convergence of the OF with an increase in the number of iterations. Figure 27b shows that there is a partial overlap of the decomposition pulses. However, this does not affect the U_{max} level. The minimization of U_{max} is achieved by equalizing the amplitudes of modes 1, 2, and 3. At an EMF of 5 V, the U_{in} level is 2.87 V (whereas in the matched case, it would tend to 2.5 V). The τ_i values are 5.4, 5.54, and 6.11 ns/m, and $\Delta\tau_i$ are 0.14 and 0.57 ns/m. In all cases, the algorithm finishes calculations at the end of a given number of iterations. To find a solution, the algorithm needs about 5000 calculations and about 37,900 s per run.

7. Discussion

1. Optimization of Protective Structures with a Circular Cross-Section

The study has shown that due to the coincidence of certain τ_i values in the MF with and without a protective shield, some pulses overlap, and the final UWB pulse attenuation decreases. This could be caused, first of all, by the fact that the electromagnetic coupling of the active conductor with the passive ones is the same. We managed to achieve CD of the exciting UWB pulse in all considered MFs when performing optimization by HS_{opt}. The total duration of the exciting UWB pulse (taking into account the partial superposition of the rise and the fall of adjacent DPs) can be increased to 0.744, 1.71, 0.249, and 0.579 ns for MFs 1–4, respectively, with the same attenuation coefficient. We have also analyzed the specific behavior of UWB pulses at the output of structures without a shield and structures with a shield. The analysis showed that in the MF with a shield, it is much more difficult to achieve CD of the output signal. This happens because DPs arrive at the end of the structures ahead of time (compared to the MF without a shield). However, complete UWB decomposition is possible through careful optimization.

2. Cascade Connection of Modal Filters

The results have shown that when the segments are cascaded, and the parameters of the structures are selected correctly, each pulse is successively decomposed into pulses of smaller amplitudes, which do not coincide with each other in time. The analysis results showed that when two segments of structures with a circular CS are connected in cascade at N = 3, a sequence of nine pulses is obtained at the output with a maximum amplitude 8.9 times less than the amplitude of the input voltage. If we add the third segment, the

pulses are also decomposed into a sequence of 27 pulses with a maximum output amplitude 25.5 times less than the U_{in}. When cascading a structure with a circular CS and an MSL at $N = 3$, a sequence of nine pulses is obtained at the output with a maximum amplitude 9.4 times less than the amplitude of the input voltage. If we add a second MF segment with a circular CS to the structure, the pulses are also decomposed into a sequence of 27 pulses with a maximum output amplitude 22.3 times less than the U_{in}. Summarizing the above, a significant improvement in the characteristics of multiconductor protective structures can be received if segment cascading is used and its parameters are selected correctly. Thus, when three segments of structures with a circular CS are connected in cascade, the output signal was attenuated by 25.5 times.

3. Parametric Optimization of Modal Filters in the Range of Real Geometric and Electrophysical Parameters

The MFs with a circular CS have been simulated and optimized in the range of real geometric and electrophysical parameters. As a result of optimization, the exciting UWB pulse was completely decomposed in all MFs with the maximum attenuation of 3.2 times (for MF 6 in the lossless simulation) and 12.4 times (for MFs 5 and 6 in the lossy simulation). Relatively equal time intervals were also achieved between DPs in MFs 5–7. Finally, acceptable path matching was ensured in all MFs after optimization. The data obtained demonstrate that the lossless optimization allowed improving the characteristics of the studied MFs according to a number of criteria. However, it is important to note the need for further lossy optimization of MFs for experimental implementation.

4. Experimental Studies of Modal Filters with a Circular Cross-Section

The results of the experiment confirm that the exciting pulse can be decomposed at the end of the active MF conductor, which was previously shown only in simulations. The MF was also studied in the frequency domain. In addition, we compared the results of computational and natural experiments in the time domain. The output voltage waveforms that we obtained experimentally and through simulation showed consistency. The measured MFs were found to have a bandwidth of 0.19–0.41 GHz, and the values of the maximum output voltage were 21.8, 27.5, and 21.1 times less than the EMF amplitude for MFs 1–3, respectively. In general, the discrepancy between the results of the experiment and lossy simulation can be explained by the following factors: loss matrices were inaccurately calculated; the influence of the frequency dependence of the relative dielectric permittivity of materials was left unaddressed; the surface-mount SMA-connectors and PCBs had inhomogeneities; the conductive media (copper on the PCB and aluminum in the MF) differed; the CS of the MF was heterogeneous along the entire length; and the values of the relative dielectric permittivity and the loss tangent, which were used in the simulation, might have deviated from the real ones. Nevertheless, the results of the experiment are comparable with the results of lossy simulations.

5. Optimization of Modal Filters by Evolutionary Strategies

The article shows the distinctive features in the optimization of an MF with a circular CS and a strip MF. Based on these features, a technique for optimizing the MF with a circular CS using the ES algorithm has been developed. The workability of the presented technique was shown in the example of optimization of 3 and 4-conductor MFs. When optimizing these MFs, 10 parameters were simultaneously optimized, and the time spent on one run, at 5000 iterations, was in the range of 17,000–40,000 s.

Finally, we present a table (Table 8) showing a comparison of MF based on strip [24–29] and cable (presented in this paper) protective structures.

Table 8. Approximate characteristics of strip and cable protective structures.

Structure	ε_r	l, m	$\Delta\tau_{min}$, ns/m	$l \cdot \Delta\tau_{min}$, ns
Strip line	4–10	0.01–1	1–2.5	0.01–2.5
Protective cable	2–5	0.5–100	0.2–1.7	0.1–170

Despite the lower ε_r value used in protective cables, the possibility of increasing their length favorably affects the mode delays in such MFs. This means that the attenuation of the UWB pulse that came to the input of such an MF will be due not only to attenuation (due to the large length) but also to its complete decomposition into a sequence of modes.

The significance and novelty of the proposed methods, in terms of the use of asymmetry in the MFs under consideration, are due to the revealed possibility of attenuating the exciting USP (because of its complete decomposition into a sequence of modes) in multiconductor cable configurations with proper optimization. Due to the ubiquitous use of cable structures, they primarily transmit interference signals, which is why the use of additional protection in them is an important task. In terms of using the optimization of the MF with a circular section by means of ES, for the first time, a technique for solving this problem was implemented and tested. Its significance, first of all, is due to the appeared possibility of correct optimization of the MF data without resorting to a time-consuming heuristic search.

8. Conclusions

We have carried out a comprehensive study of a new design of protective devices with circular CS (protective cables) for protection against UWB pulses. Multiconductor structures with 2–5 conductors were considered in their design with and without a shield. The study demonstrated the disadvantages of using symmetric protective cable configurations. To eliminate these disadvantages, breaking the symmetry of the traditional (symmetric) cable configurations was performed. This is performed through their simulation, multivariate analysis, and optimization by HS_{opt}; also ES were performed. The optimization was performed according to the amplitude and time criteria. The amplitude criterion was employed to minimize the maximum voltage level at the output of the structures. The time criterion was necessary to maximize the duration of the interfering signal. An improvement in the protective characteristics was observed when symmetry was broken and asymmetry was introduced into the CS of the structures under consideration. The optimization results ensured the increase in the duration and final attenuation of the exciting UWB pulse. Improving the characteristics of such structures is possible through their cascade connection, both among themselves and with strip protective devices. We also presented the results of parametric optimization of such structures in the range of real (used in practice) geometric and electrical parameters in terms of amplitude, time, and matching criteria. The results of the experiment included the development and creation of layouts for the structures with a circular CS of three types: a circular 3-conductor cable, a flat 3-conductor cable, and a circular 4-conductor cable. We managed to confirm the possibility of the exciting UWB pulse decomposition in protective structures with a circular CS, which was previously shown only in simulations.

Thus, the expediency of further in-depth study of the considered MFs is shown in terms of creating a prototype MF and its experimental studies. It also seems relevant to study the possibility of multicriteria optimization of the considered MFs using global optimization methods.

Supplementary Materials: The following are available online https://www.mdpi.com/article/10.3390/sym14061228/s1, Table S1: Voltages (U_i, mV) and delays (t_i, ns) of pulses along the active conductor of CC 1, Table S2: Voltages (U_i, mV) and delays (t_i, ns) of pulses along the active conductor of CC 2, Table S3: Voltages (U_i, mV) and delays (t_i, ns) of pulses along the active conductor of CC 3, Table S4: Voltages (U_i, mV) and delays (t_i, ns) of pulses along the active conductor of CC 4, Table S5: Optimization results for a 3-conductor MF with a circular CS, Table S6: Optimization results for

a 4-conductor MF with a circular CS, Table S7: Optimization results for a 3-conductor MF with a circular CS with insulation around the conductors.

Author Contributions: Conceptualization, T.R.G.; validation, A.O.B.; formal analysis, A.O.B.; investigation, A.O.B., N.O.V., and V.O.G.; writing—original draft preparation, N.O.V. and V.O.G.; writing—review and editing, A.O.B. and T.R.G.; supervision, T.R.G. All authors have read and agreed to the published version of the manuscript.

Funding: The reported study was funded by the Russian Federation President grant MK-900.2022.4 and the Ministry of Science and Higher Education of the Russian Federation project FEWM-2022-0001.

Institutional Review Board Statement: Not applicable.

Informed Consent Statement: Not applicable.

Data Availability Statement: Not applicable.

Acknowledgments: The authors sincerely appreciate all valuable comments and suggestions from the reviewers, which helped us to improve the quality of the paper.

Conflicts of Interest: The authors declare no conflict of interest.

References

1. Gizatullin, Z.M.; Gizatullin, R.M. Investigation of the immunity of computer equipment to the power-line electromagnetic interference. *J. Comm. Technol. Electron* **2016**, *61*, 546–550. [CrossRef]
2. Mankov, P.N.; Melnikov, A.A.; Popov, M.G.; Novikov, A.V.; Bessolitsin, A.V. Ensuring Electromagnetic Compatibility of Control and Measuring Cables in Case of Phase-Shielded Conductor-Induced Interference in Non-Stationary Modes. In Proceedings of the 2021 IEEE Conference of Russian Young Researchers in Electrical and Electronic Engineering (ElConRus), St. Petersburg, Russia; Moscow, Russia, 26–29 January 2021; pp. 1269–1274.
3. Vanin, V.; Bulychov, A.; Popov, M.; Vasilyeva, O.; Shakhova, M. About influence of non-sinusoidal currents and voltages on the amount of the electric energy. *MATEC Web Conf.* **2018**, *245*, 06009. [CrossRef]
4. Vanin, V.; Bulychov, A.; Popov, M.; Vasilyeva, O.; Shakhova, M. Measurement of currents and voltages non-sinusoidal parameters in power supply systems with rectifier load. *MATEC Web Conf.* **2018**, *245*, 06007. [CrossRef]
5. Adamyan, Y.; Krivosheev, S.; Magazinov, S. Experimental study of alternating magnetic field in laminated ferromagnetic core. *MATEC Web Conf.* **2018**, *245*, 07001. [CrossRef]
6. Krivosheev, S.I.; Magazinov, S.G.; Shneerson, G.A. Specific features of the nonlinear diffusion of a strong pulsed magnetic field near the conductor edge. *Tech. Phys. Lett.* **2019**, *45*, 100–104. [CrossRef]
7. Popov, M.G.; Bocharov, Y.N.; Halilov, F.H.; Gurevich, E.I.; Popov, V.V.; Akhmetov, T.R. Multifunctional electronic devices protected and automatic of modern electricity system. *IOP Conf. Ser. Earth Environ. Sci.* **2019**, *337*, 12017. [CrossRef]
8. Zelenin, A.S. Development and implementation experience of microprocessor emulators for cyber-physical AVR testing complexes. In Proceedings of the 2019 IEEE Conference of Russian Young Researchers in Electrical and Electronic Engineering (EIConRus), Saint Petersburg, Russia; Moscow, Russia, 28–31 January 2019; Volume 8657237, pp. 752–756.
9. Popov, M.G.; Tarasevich, M.D.; Bogdanov, A.V.; Bazlov, D.A.; Gushin, M.V. Method and algorithm of fault detecting in circuits of the thyristor excitation system of synchronous machines. In Proceedings of the IEEE 2020 Conference of Russian Young Researchers in Electrical and Electronic Engineering (EIConRus), Saint Petersburg, Russia; Moscow, Russia, 27–30 January 2020; pp. 835–840.
10. Krivosheev, S.I.; Magazinov, S.G.; Adamyan, Y.E.; Alekseev, D.I.; Manzuk, M.V. Uniaxial high strain rate tension with the use of magnetic pulse method. In Proceedings of the IEEE Conference of Russian Young Researchers in Electrical and Electronic Engineering (EIConRus), Saint Petersburg, Russia; Moscow, Russia, 27–30 January 2020; pp. 1082–1086.
11. Leuchter, J.; Dong, Q.H.; Boril, J.; Blasch, E. Electromagnetic immunity of aircraft wireless and cables from electromagnetic interferences. In Proceedings of the IEEE/AIAA 36th Digital Avionics Systems Conference (DASC), St. Petersburg, FL, USA, 17–21 September 2017; pp. 1–6.
12. Zhang, Z.; Liu, H.; Xue, Z.; Abdo, A.M.A.; Yu, D.; Yang, Z.; Wen, C.; Lu, Y.; Yan, M.; Huang, Y. The Investigation of the Lightning Overvoltage of Secondary Cable of Substation. In Proceedings of the IEEE International Conference on High Voltage Engineering and Application (ICHVE), Beijing, China, 6–10 September 2020; pp. 1–4.
13. Ma, H.; Zhang, W.; Liu, X. Study of the impaction by lightning strike on communication cable based on time-domain finite element method. In Proceedings of the XXXIInd General Assembly and Scientific Symposium of the International Union of Radio Science (URSI GASS), Montreal, QC, Canada, 19–26 August 2017; pp. 1–4.
14. Tanaka, H.; Baba, Y.; Barbosa, C.F.; Tsuboi, T.; Okabe, S. Protective effect of shield wires against direct lightning flashes to buried cables. *IEEE Trans. Power Deliv.* **2018**, *33*, 1628–1635. [CrossRef]

15. Yafei, H.; Yu, Z.; Hui, Z. A non-terminal points grounding method of shielded cable for electromagnetic pulse protection. In Proceedings of the IEEE 5th International Symposium on Electromagnetic Compatibility (EMC-Beijing), Beijing, China, 28–31 October 2017; pp. 1–5.
16. Pornin, C.; Vuong, T.P.; Xavier, P.; Angenieux, G. A Novel Approach on Multi-Shielded Coaxial Cable Immunity Assessment Based on Electromagnetism Simulation. In Proceedings of the Asia-Pacific Microwave Conference (APMC), Kyoto, Japan, 6–9 November 2018; pp. 387–389.
17. Benato, R.; Dambone Sessa, S.; Viafora, N.; Palone, F. Impact of protective structures on EHV cable transient behaviour: Comparison between FEM, EMTP and measurements. In Proceedings of the AEIT International Annual Conference (AEIT), Capri, Italy, 5–7 October 2016; pp. 1–6.
18. Lee, S.R.; Lee, J.; Yoon, J.; Kang, Y.; Hur, J. Impact of 154-kV HTS Cable to Protection Systems of the Power Grid in South Korea. *IEEE Trans. Ind. Appl. Supercond.* **2016**, *26*, 5402404. [CrossRef]
19. Bulson, J.M. Low-impedance cable for parallel-connected surge protective devices. *IEEE Trans. Power Deliv.* **1995**, *10*, 1816–1821. [CrossRef]
20. Yan, X.; Wu, C.; Zhang, D.; Jin, S.; Wu, S.; Fan, J.; Hwaang, C. EMI investigation and mitigation of flexible flat cables and connectors. In Proceedings of the IEEE International Joint EMC/SI/PI and EMC Europe Symposium, Raleigh, NC, USA, 26 July–13 August 2021; pp. 515–519.
21. Gizatullin, Z.; Shkinderov, M. Research of Electromagnetic Interference in the Power Supply Network of the Access Monitoring and Control System. In Proceedings of the 2021 International Conference on Industrial Engineering, Applications and Manufacturing (ICIEAM), Sochi, Russia, 17–21 May 2021; pp. 20–524.
22. Gizatullin, Z.M.; Gizatullin, R.M.; Nuriev, M.G. Prediction of Noise Immunity of Computing Equipment under the Influence of Electromagnetic Interference through the Metal Structures of Building by Physical Modeling. In Proceedings of the IEEE Conf. of Russian Young Researchers in Electrical and Electronic Engineering (EIConRus), St. Petersburg, Russia; Moscow, Russia, 27–30 January 2020; pp. 120–123.
23. Nuriev, M.G.; Gizatullin, R.M.; Gizatullin, Z.M. Physical Modeling of Electromagnetic Interferences in the Electronic Devices at Direct Impact of Lightning on Protection System of Building. In Proceedings of the XIV International Scientific-Technical Conference on Actual Problems of Electronics Instrument Engineering (APEIE), Novosibirsk, Russia, 2–6 October 2018; pp. 355–358.
24. Belousov, A.O.; Chernikova, E.B.; Samoylichenko, M.A.; Medvedev, A.V.; Nosov, A.V.; Gazizov, T.R.; Zabolotsky, A.M. From Symmetry to Asymmetry: The Use of Additional Pulses to Improve Protection against Ultrashort Pulses Based on Modal Filtration. *Symmetry* **2020**, *12*, 1117. [CrossRef]
25. Gazizov, A.T.; Zabolotsky, A.M.; Gazizov, T.R. UWB pulse decomposition in simple printed structures. *IEEE Trans. Electromagn. Compat.* **2016**, *58*, 1136–1142. [CrossRef]
26. Belousov, A.; Medvedev, A.; Chernikova, E.; Gazizov, T.; Zabolotsky, A. Switching Order after Failures in Symmetric Protective Electrical Circuits with Triple Modal Reservation. *Symmetry* **2021**, *13*, 1074. [CrossRef]
27. Chernikova, E.B.; Belousov, A.O.; Gazizov, T.R.; Zabolotsky, A.M. Using reflection symmetry to improve the protection of radio-electronic equipment from ultrashort pulses. *Symmetry* **2019**, *11*, 883. [CrossRef]
28. Gazizov, T.; Zabolotsky, A.; Samotin, I.; Melkozerov, A. Simple and free mitigation of short pulse lightning effects by flat power cables. In Proceedings of the 30th International Conference on Lightning Protection (ICLP), Cagliari, Italy, 13–17 September 2010; pp. 1–3.
29. Gazizov, T.; Zabolotsky, A. New approach to EMC protection. In Proceedings of the 18th International Zurich Symposium on Electromagnetic Compatibility, Munich, Germany, 24–28 September 2007; pp. 273–276.
30. Belousov, A.O.; Zabolotsky, A.M. Modal decomposition of an ultrashort pulse in a multiconductor transmission line with circular symmetry. In Proceedings of the 11th International Scientific and Practical Conference Electronic Instruments and Control Systems, Tomsk, Russia, 25–26 November 2015; volume 2, pp. 14–18.
31. Belousov, A.O.; Vlasova, N.O. Parametric optimization of the cables with the modal filtration effect. *J. Phys. Conf. Ser.* **2021**, *1862*, 012004. [CrossRef]
32. Belousov, A.O.; Gazizov, T.T. Complete ultrashort pulse decomposition in modal filters with circular symmetry. *IOP Conf. Ser. Mater. Sci. Eng.* **2020**, *862*, 52050. [CrossRef]
33. Mitchell, M.; Holland, J.; Forrest, S. When will a genetic algorithm outperform hill climbing? In *Handbook of Metaheuristics*, 1st ed.; Glover, F., Kochenberger, G., Eds.; Springer: Boston, MA, USA, 2003; Volume 1, pp. 51–58.
34. Mittra, R.; Chakravarty, S.; Yeo, J. Application of micro-genetic algorithm (MGA) to a class of electromagnetic analysis and synthesis problems. *IEEE Antennas Propag. Soc. Int. Symp.* **2002**, *1*, 306–309.
35. Freisleben, B.; Merz, P. A genetic local search algorithm for solving symmetric and asymmetric traveling salesman problems. In Proceedings of the IEEE 1996 International Conference on Evolutionary Computation, Nagoya, Japan, 20–22 May 1996; pp. 616–621.
36. Gazizov, R.R.; Zabolotsky, A.M.; Gazizov, R.R. Use of evolution strategy in identifying the worst case effects of ultrashort pulse propagation in PCB bus of spacecraft autonomous navigation system. In Proceedings of the Int. Siberian Conf. on Control and Communications (SIBCON 2018), Moscow, Russia, 14–16 March 2018; pp. 1–4.
37. Kuksenko, S.P. Preliminary results of TUSUR University project for design of spacecraft power distribution network: EMC simulation. *IOP Conf. Ser. Mater. Sci. Eng.* **2019**, *560*, 012110. [CrossRef]

38. Gazizov, T.R.; Sagiyeva, I.Y.; Kuksenko, S.P. Solving the complexity problem in the electronics production process by reducing the sensitivity of transmission line characteristics to their parameter variations. *Complexity* **2019**, *2019*, 6301326. [CrossRef]
39. Matthaei, G.L.; Chinn, G.C. Approximate calculation of the high-frequency resistance matrix for multiple coupled lines. In Proceedings of the 1992 IEEE MTT-S Microwave Symposium Digest, Albuquerque, NM, USA, 1–5 June 1992; pp. 1353–13540.
40. Gordeyeva, V.O.; Belousov, A.O. Optimization of a broad-side coupling modal filter by evolutionary strategy algorithm with setting the ranges of the optimization parameters. *J. Phys. Conf. Ser.* 2021; *accepted*.
41. Belousov, A.O.; Vlasova, N.O. Parametric Optimization of Shielded Multiconductor Modal Filters with Circular Cross Section. In Proceedings of the 22st International Conference of Young Specialists on Micro/Nanotechnologies and Electron Devices EDM, Altai, Russia, 30 June–4 July 2021; pp. 153–157.
42. Gazizov, T.; Samotin, I.; Zabolotsky, I.; Melkozerov, A. Design of printed modal filters for computer network protection. In Proceedings of the 30th International Conference on Lightning Protection (ICLP), Cagliari, Italy, 13–17 September 2010; pp. 1–3.
43. Belousov, A.O.; Gazizov, T.R. Systematic approach to optimization for protection against intentional ultrashort pulses based on multiconductor modal filters. *Complexity* **2018**, *2018*, 5676504. [CrossRef]
44. Belousov, A.O.; Vlasova, N.O. Optimization of protective cables in the range of real geometric parameters. *J. Phys. Conf. Ser.* 2021; *accepted*.